

THESIS

WEAK GALERKIN FINITE ELEMENT METHODS FOR THE DARCY EQUATION

Submitted by

Zhuoran Wang

Department of Mathematics

In partial fulfillment of the requirements

For the Degree of Master of Science

Colorado State University

Fort Collins, Colorado

Spring 2018

Master's Committee:

Advisor: Jianguo (James) Liu

Co-Advisor: Simon Tavener

Tammy Donahue

Copyright by Zhuoran Wang 2017
All Rights Reserved

ABSTRACT

WEAK GALERKIN FINITE ELEMENT METHODS FOR THE DARCY EQUATION

The Darcy equation models pressure-driven flow in porous media. Because of the importance of ground water flow in oil recovery and waste mitigation, several types of numerical methods have been developed for solving the Darcy equation, such as continuous Galerkin finite element methods (CGFEMs) and mixed finite element methods (MFEMs).

This thesis describes the lowest-order weak Galerkin (WG) finite element method to solve the Darcy equation and compares it to those well-known methods. In this method, we approximate the pressure by constants inside elements and on edges. Pressure values in interiors and on edges might be different. The discrete weak gradients specified in the local Raviart-Thomas spaces are used to approximate the classical gradients.

The WG finite element method has nice features, e.g., locally mass conservation, continuous normal fluxes and easy implementation. Numerical experiments on quadrilateral and hybrid meshes are presented to demonstrate its good approximation and expected convergence rates. We discuss the extension of WG finite element methods to three-dimensional domains.

TABLE OF CONTENTS

ABSTRACT	ii
Chapter 1: Introduction	1
1.1 Background	1
1.2 Outline	2
Chapter 2: Existing Finite Element Methods for the Darcy Equation	3
2.1 Continuous Galerkin Finite Element Methods	3
2.1.1 CGFEMs on Triangular Meshes	5
2.1.2 CGFEMs on Rectangular Meshes	9
2.1.3 Features of CGFEMs	10
2.2 Mixed Finite Element Methods	11
2.2.1 Mixed Formulation	11
2.2.2 Raviart-Thomas Elements (RT_0, P_0) on Triangles	12
2.2.3 Raviart-Thomas Element $(RT_{[0]}, Q_0)$ on Rectangles	16
2.2.4 Features of MFEMs	16
Chapter 3: WGFEMs for Darcy on Two-Dimensional Meshes	18
3.1 Lowest Order WG Finite Elements on Triangles and Quadrilaterals	20
3.1.1 Triangular Elements	20
3.1.2 Quadrilateral Elements	23
3.2 WGFEMs for Darcy	26
3.3 Properties and Convergence	27
3.3.1 Local Mass Conservation	27
3.3.2 Normal Flux Continuity	28
3.3.3 Convergence	29
3.4 Lowest Order WG Scheme for the Darcy Equation	30

3.5	Numerical Results on Quadrilateral Meshes	38
3.6	Lowest Order WGFEMs on Hybrid Meshes	41
Chapter 4: WGFEMs on Hexahedral Meshes		43
4.1	WG $(Q_0, Q_0; RT_{[0]})$ Elements on Hexahedra	43
4.2	Lowest Order WG Scheme for Darcy on Hexahedra	44
Chapter 5: WGFEMs for Elasticity		48
Chapter 6: Conclusion		53
6.1	Other Combinations for WG Elements	53
6.1.1	WG $(Q_1, P_1; RT_{[0]})$ Elements on Quadrilaterals	53
6.1.2	WG $(Q_0, Q_0; RT_{[1]})$ Elements on Quadrilaterals	56
6.2	Conclusion	58
Bibliography		60

CHAPTER 1

INTRODUCTION

1.1 BACKGROUND

In 1856, the French engineer Henry Darcy formulated the Darcy's law for flow in a porous medium based on his experiments of water flowing through beds of sand. In Figure (1.1), Q

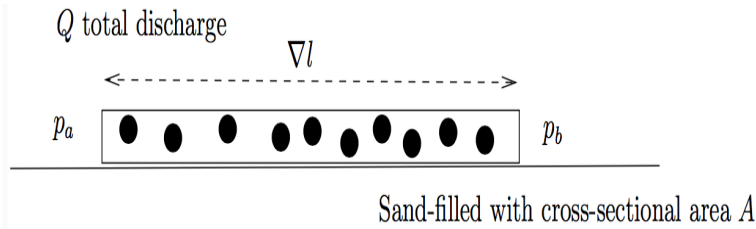


Figure 1.1: Darcy's law

(m^3/s) is the total discharge, A (m^2) is the cross-sectional area to flow, $(p_b - p_a)$ (pascals) is the total pressure drop, ∇l (m) is the length over the pressure drop. Darcy's law was introduced by Darcy [14] and then refined by Morris Muskat. It becomes

$$Q = -\frac{\kappa A(p_b - p_a)}{\mu \nabla l}, \quad (1.1)$$

where κ (m^2) is the permeability of the medium, μ ($\text{Pa}\cdot\text{s}$) is the viscosity of fluid, the negative sign comes from the reason that the fluid flows from higher pressure to lower pressure.

Darcy's law has become an important tool in analysis of the ground water flow and is widely used in the areas of hydrodynamics, oil recovery, chemical engineering and many other engineering fields. The Darcy equation coupled with the elasticity equation has been used to describe flow in a poroelastic medium.

1.2 OUTLINE

This thesis concentrates on a typical boundary value problem defined by the Darcy equation on a domain Ω . The Darcy equation is formulated as

$$\begin{cases} \nabla \cdot (-\mathbf{K}\nabla p) \equiv \nabla \cdot \mathbf{u} = f, & \mathbf{x} \in \Omega, \\ p = p_D, & \mathbf{x} \in \Gamma^D, \quad \mathbf{u} \cdot \mathbf{n} = u_N, & \mathbf{x} \in \Gamma^N, \end{cases} \quad (1.2)$$

where $\Omega \subset \mathbb{R}^n (n = 2, 3)$ is a bounded domain. In the context of the flow of a fluid through a porous medium, p is the pressure, \mathbf{K} is a permeability tensor, $\mathbf{u} = -\mathbf{K}\nabla p$ is the Darcy velocity which is the flow per unit cross sectional area of the porous medium, f is the source term, p_D, u_N are respectively Dirichlet and Neumann boundary data.

Several methods have been developed for solving the Darcy equation, such as continuous Galerkin finite element methods (CGFEMs) and mixed finite element methods (MFEMs) [7, 10, 14, 32]. For both these two methods, we ultimately need to solve a large-scale linear system. Although CGFEMs have fewer unknowns, they are also known to lack local mass conservation and flux continuity. MFEMs solve the unknown pressure and the velocity simultaneously, but they need to satisfy the inf-sup condition and result in an indefinite linear system. Here, we use the weak Galerkin finite element methods (WGFEMs) introduced in [28] to solve the Darcy equation.

This thesis is organized as follows. In Chapter 2, we present the existing finite element methods, CGFEMs and MFEMs, for solving the Darcy equation. In Chapter 3, WGFEMs are presented in detail, such as the construction of weak Galerkin finite element schemes on quadrilateral and triangular meshes and numerical experiments. Chapter 4 discusses the WG method for three-dimensional flows. Chapter 5 describes the future work for WGFEMs and Chapter 6 concludes this thesis.

CHAPTER 2

EXISTING FINITE ELEMENT METHODS FOR THE DARCY EQUATION

There are several finite element methods for solving the Darcy equation, including CGFEMs, discontinuous Galerkin finite element methods (DGFEMs), WGFEMs and MFEMs. In this chapter, we focus on describing two well-known finite element methods, CGFEMs and MFEMs [8, 12].

2.1 CONTINUOUS GALERKIN FINITE ELEMENT METHODS

The Darcy equation on a bounded polygonal domain $\Omega \in \mathbb{R}^n (n = 2, 3)$ is formulated as

$$\begin{cases} \nabla \cdot (-\mathbf{K}\nabla p) \equiv \nabla \cdot \mathbf{u} = f, & \mathbf{x} \in \Omega, \\ p = p_D, & \mathbf{x} \in \Gamma^D, \quad \mathbf{u} \cdot \mathbf{n} = u_N, & \mathbf{x} \in \Gamma^N. \end{cases} \quad (2.1)$$

Here, for simplicity, we take a homogeneous Dirichlet boundary condition on the entire boundary of a two-dimensional domain.

We define the spaces for scalar-valued function

$$H^1(\Omega) = \{p \in L^2(\Omega), \nabla p \in L^2(\Omega)\}, \quad (2.2)$$

$$H_0^1(\Omega) = \{p \in H^1(\Omega) : p|_{\partial\Omega} = 0\}. \quad (2.3)$$

The Ritz-Galerkin form of the Darcy equation (1.2) is

$$\int_{\Omega} \nabla \cdot (-\mathbf{K}\nabla p)q = \int_{\Omega} fq, \quad \forall q \in H_0^1(\Omega), \quad (2.4)$$

where q is a test function in the space, and $q = 0$ on the Dirichlet boundaries Γ^D . Through integration by parts, the left hand side becomes

$$\int_{\Omega} \nabla \cdot (-\mathbf{K}\nabla p)q = - \int_{\partial\Omega} q(\mathbf{K}\nabla p) \cdot \mathbf{n} + \int_{\Omega} \mathbf{K}\nabla p \cdot \nabla q. \quad (2.5)$$

We define the space $V = H_0^1(\Omega)$. So the variational form of the Darcy equation (1.2) by CGFEMs is

$$\int_{\Omega} \mathbf{K}\nabla p \cdot \nabla q = \int_{\Omega} f q, \quad \forall q \in V. \quad (2.6)$$

Let \mathcal{E}_h be a collection of elements E , and $\Omega = \cup_{E \in \mathcal{E}_h} E$. The boundary term of the right hand side of (2.5) vanishes because the test function $q = 0$ on the Dirichlet boundaries and there is no Neumann boundary condition. We define the finite dimensional subspace $V_h = \text{Span}\{\Phi_1, \Phi_2, \dots, \Phi_n\}$, and $V_h \subset V$. The primal pressure is $p_h = \sum_{j=1}^n c_j \Phi_j$, and the finite element scheme for the Darcy equation on V_h is

$$\int_{\Omega} \mathbf{K}\nabla p_h \cdot \nabla q = \int_{\Omega} f q, \quad \forall q \in V_h, \quad (2.7)$$

$$\int_{\Omega} \mathbf{K}\nabla \left(\sum_{j=1}^n c_j \Phi_j \right) \cdot \nabla \Phi_i = \int_{\Omega} f \Phi_i, \quad 1 \leq i \leq n, \quad (2.8)$$

So for the Darcy equation with Dirichlet and Neumann boundary conditions, we have the following scheme:

$$\mathcal{A}_h(p_h, q) = \mathcal{F}(q), \quad (2.9)$$

where p_h is the numerical pressure, q is the test function in the finite element space, and $q = 0$ on Γ^D , and $\mathcal{A}_h(p_h, q)$ is the bilinear form

$$\mathcal{A}_h(p_h, q) := \sum_{E \in \mathcal{E}_h} \int_E \mathbf{K}\nabla p_h \cdot \nabla q, \quad \forall q \in V_h, \quad (2.10)$$

and $\mathcal{F}(q)$ is the linear form

$$\mathcal{F}(q) := \sum_{E \in \mathcal{E}_h} \int_E f q - \sum_{\gamma \in \Gamma_h^N} \int_{\gamma} u_N q, \quad \forall q \in V_h. \quad (2.11)$$

2.1.1 CGFEMs on Triangular Meshes

For the basis functions ϕ_i in each element, we use \mathcal{P} -type polynomials. For example, we use \mathcal{P}_1 -type polynomial, which is the polynomial with the form of $x^i y^j$ and $(i + j) \leq 1$. For CGFEMs with \mathcal{P}_1 -type polynomial, we denote it as CGP1. Let \mathcal{T}_h be a triangular mesh. On each triangular element T , the basis functions ϕ_1, ϕ_2, ϕ_3 are defined on the element using locations of three vertices, and

$$\phi_1 = \frac{|T_1|}{|T|} = \frac{\begin{vmatrix} 1 & x & y \\ 1 & x_2 & y_2 \\ 1 & x_3 & y_3 \end{vmatrix}}{\begin{vmatrix} 1 & x_1 & y_1 \\ 1 & x_2 & y_2 \\ 1 & x_3 & y_3 \end{vmatrix}}, \quad \phi_2 = \frac{|T_2|}{|T|} = \frac{\begin{vmatrix} 1 & x_1 & y_2 \\ 1 & x & y \\ 1 & x_3 & y_3 \end{vmatrix}}{\begin{vmatrix} 1 & x_1 & y_1 \\ 1 & x_2 & y_2 \\ 1 & x_3 & y_3 \end{vmatrix}}, \quad \phi_3 = \frac{|T_3|}{|T|} = \frac{\begin{vmatrix} 1 & x_1 & y_1 \\ 1 & x_2 & y_2 \\ 1 & x & y \end{vmatrix}}{\begin{vmatrix} 1 & x_1 & y_1 \\ 1 & x_2 & y_2 \\ 1 & x_3 & y_3 \end{vmatrix}}, \quad (2.12)$$

where $|T|$ is the scalar value of each element's area, $|T_i|$ is a function of x and y and it is

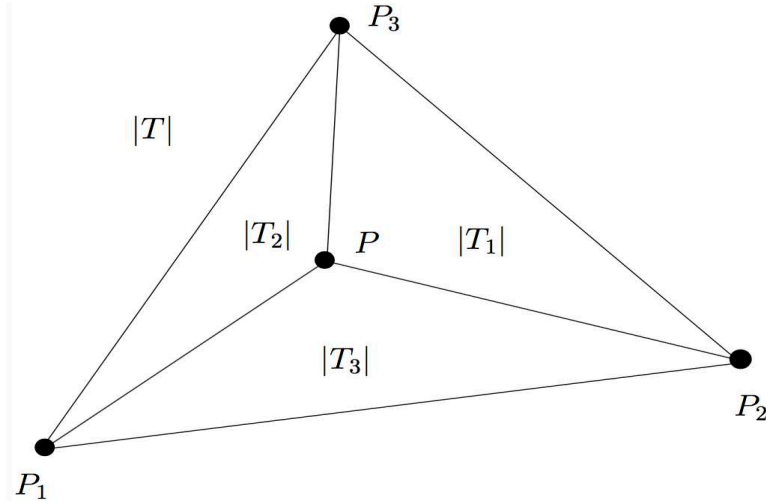


Figure 2.1: Triangle geometric information used for CGFEMs

the area of the small triangle, shown in Figure (2.1), and $\phi_i(P_j) = \delta_{ij}$, $P_j (j = 1, 2, 3)$ are vertices of the element.

In implementation, the global basis functions $\Phi_i (i = 1, 2, \dots, n)$ will be the “gluing-together” of the local basis functions ϕ_i . For solving the weak form of the Darcy equation on a whole triangular mesh, the left hand side of the finite element scheme is a product of the global stiffness matrix and the array of the coefficients. So we calculate the element stiffness matrices on all local elements and then assemble them into the global stiffness matrix.

The element stiffness matrix on each element is

$$\begin{bmatrix} \int_T \nabla \phi_1 \cdot \nabla \phi_1 & \int_T \nabla \phi_1 \cdot \nabla \phi_2 & \int_T \nabla \phi_1 \cdot \nabla \phi_3 \\ \int_T \nabla \phi_2 \cdot \nabla \phi_1 & \int_T \nabla \phi_2 \cdot \nabla \phi_2 & \int_T \nabla \phi_2 \cdot \nabla \phi_3 \\ \int_T \nabla \phi_3 \cdot \nabla \phi_1 & \int_T \nabla \phi_3 \cdot \nabla \phi_2 & \int_T \nabla \phi_3 \cdot \nabla \phi_3 \end{bmatrix}. \quad (2.13)$$

It is easy to derive

$$\nabla \phi_1 = \frac{1}{2|T|} (y_2 - y_3, x_3 - x_2), \quad (2.14)$$

$$\nabla \phi_2 = \frac{1}{2|T|} (y_3 - y_1, x_1 - x_3), \quad (2.15)$$

$$\nabla \phi_3 = \frac{1}{2|T|} (y_1 - y_2, x_2 - x_1). \quad (2.16)$$

According to Equation (2.10), the global stiffness matrix is

$$\begin{bmatrix} \int_{\Omega} \nabla \Phi_1 \cdot \nabla \Phi_1 & \int_{\Omega} \nabla \Phi_1 \cdot \nabla \Phi_2 & \cdots & \int_{\Omega} \nabla \Phi_1 \cdot \nabla \Phi_n \\ \int_{\Omega} \nabla \Phi_2 \cdot \nabla \Phi_1 & \int_{\Omega} \nabla \Phi_2 \cdot \nabla \Phi_2 & \cdots & \int_{\Omega} \nabla \Phi_2 \cdot \nabla \Phi_n \\ \vdots & & & \\ \int_{\Omega} \nabla \Phi_n \cdot \nabla \Phi_1 & \int_{\Omega} \nabla \Phi_n \cdot \nabla \Phi_2 & \cdots & \int_{\Omega} \nabla \Phi_n \cdot \nabla \Phi_n \end{bmatrix}, \quad (2.17)$$

which is a symmetric non-singular matrix. Then assemble the element stiffness matrices to

get the global stiffness matrix (2.17),

$$A(\nabla\Phi_i, \nabla\Phi_j) = \sum_{T \in \mathcal{T}_h} A_K(\phi_i, \phi_j), \quad (2.18)$$

where $A_K(\phi_i, \phi_j) = \int_T \nabla\phi_i \cdot \nabla\phi_j$. That is, we compute the global stiffness matrix A by computing the element stiffness matrix first and then sum up contributions from all other related triangles.

Global basis functions are defined in the nodal orientation. On a node of the triangular mesh, it has a support which is the union of triangles around it. If Φ_i, Φ_j don't interact in a support, $(\nabla\Phi_i, \nabla\Phi_j) = 0$. So the global stiffness matrix is a sparse symmetric non-singular matrix. The left hand side of the weak form on the domain is a linear system

$$\begin{bmatrix} \int_{\Omega} \nabla\Phi_1 \cdot \nabla\Phi_1 & \int_{\Omega} \nabla\Phi_1 \cdot \nabla\Phi_2 & \cdots & \int_{\Omega} \nabla\Phi_1 \cdot \nabla\Phi_n \\ \int_{\Omega} \nabla\Phi_2 \cdot \nabla\Phi_1 & \int_{\Omega} \nabla\Phi_2 \cdot \nabla\Phi_2 & \cdots & \int_{\Omega} \nabla\Phi_2 \cdot \nabla\Phi_n \\ & & \vdots & \\ \int_{\Omega} \nabla\Phi_n \cdot \nabla\Phi_1 & \int_{\Omega} \nabla\Phi_n \cdot \nabla\Phi_2 & \cdots & \int_{\Omega} \nabla\Phi_n \cdot \nabla\Phi_n \end{bmatrix} \begin{bmatrix} c_1 \\ c_2 \\ \vdots \\ c_n \end{bmatrix}. \quad (2.19)$$

The right hand side is an array of integrations of source term f and the basis functions of the finite dimensional space. It is the same way of assembling the right hand side of Equation (2.8),

$$\int_{\Omega} f\Phi_i = \sum_{T \in \mathcal{T}_h} \int_T f\phi_j, \quad (2.20)$$

where $\sum_{T \in \mathcal{T}_h} \int_T f\phi_j$ is calculated by adding up contributions to Φ_i from local triangles.

When we calculate the right hand side, we use the Gaussian quadrature, which is the sum of multiplications of function values on quadrature points and weights, to approximate definite integrals. For example, on a one dimensional integral, $\int_{-1}^1 f(x)$, the length of this

interval is 2, applying Gaussian quadrature, it becomes

$$\int_{-1}^1 f(x) dx = 2 \sum_{i=1}^n f(x_i) w_i,$$

$x_i (i = 1, \dots, n)$ are Gaussian quadrature points, w_i are weights of the points. On an arbitrary line interval $[a, b]$, $x \in [a, b]$, we change the variable x to be $t \in [-1, 1]$, $x = \frac{a+b}{2} + \frac{b-a}{2}t$, so the integral becomes

$$\int_a^b g(x) dx = \int_{-1}^1 f(t) \frac{b-a}{2} dt.$$

As for a two dimensional integral, $\int_T f dT$, on a triangular element T , by the Gaussian quadrature, we derive

$$\int_T f dT \approx |T| \sum_{k=1}^N w_k f(\alpha_k P_1 + \beta_k P_2 + \gamma_k P_3), \quad (2.21)$$

where α, β, γ are barycentric coordinates of the quadrature points on triangles, P_1, P_2, P_3 are three vertices of T ,

$$\alpha = \frac{|T_1|}{|T|}, \quad \beta = \frac{|T_2|}{|T|}, \quad \gamma = \frac{|T_3|}{|T|}, \quad (2.22)$$

they are the same as local basis functions ϕ_1, ϕ_2, ϕ_3 . $(\alpha_k P_1 + \beta_k P_2 + \gamma_k P_3) = P$ is a quadrature point in the element, $w_k (k = 1, \dots, N)$ are weights of the quadrature points, N is the number of the Gaussian quadrature points on the element.

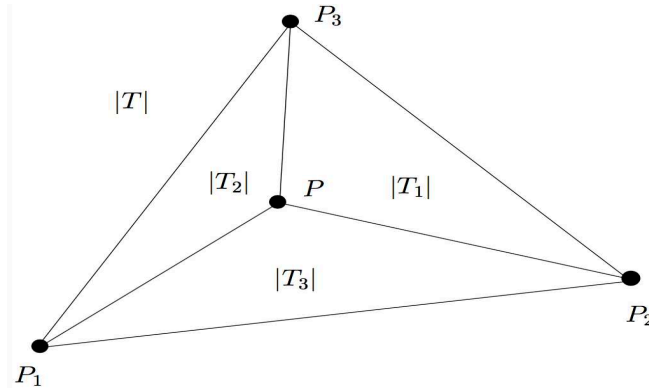


Figure 2.2: Triangle geometric information for barycentric coordinates

2.1.2 CGFEMs on Rectangular Meshes

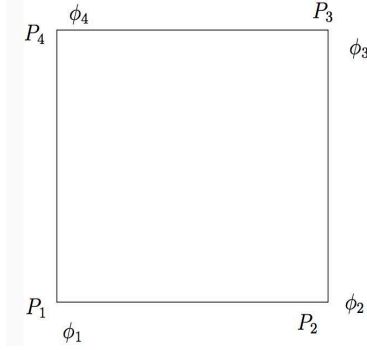


Figure 2.3: Rectangle geometric information for basis functions

Solving the Darcy equation by CGFEMs on rectangles is similar to solving the Darcy equation by CGFEMs on triangles. On each rectangle, there are four basis functions $\phi_1, \phi_2, \phi_3, \phi_4$, which are defined on the element E using the locations of four vertices. For example, on an arbitrary rectangular element $E = [x_1, x_2] \times [y_1, y_2]$, we use the \mathcal{Q}_1 -type polynomial, which means that the polynomial is with the form $x^i y^j (i, j \leq 1)$, and $\phi_i(P_j) = \delta_{ij}$,

$$\begin{aligned} \phi_1 &= \frac{(x_2-x)(y_2-y)}{(x_2-x_1)(y_2-y_1)}, & \phi_2 &= \frac{(x-x_1)(y_2-y)}{(x_2-x_1)(y_2-y_1)}, \\ \phi_3 &= \frac{(x-x_1)(y-y_1)}{(x_2-x_1)(y_2-y_1)}, & \phi_4 &= \frac{(x_2-x)(y-y_1)}{(x_2-x_1)(y_2-y_1)}, \end{aligned} \quad (2.23)$$

where (x, y) is a point inside the element. The components of gradients of these basis functions are no longer constants. We then use these basis functions on each element to construct the element stiffness matrix,

$$\begin{aligned} & [\langle \nabla \phi_i, \nabla \phi_j \rangle_E]_{1 \leq i, j \leq 4} \\ = & \left(\frac{y_2-y_1}{x_2-x_1} \right) \frac{1}{6} \begin{bmatrix} 2 & -2 & -1 & 1 \\ -2 & 2 & 1 & -1 \\ -1 & 1 & 2 & -2 \\ 1 & -1 & -2 & 2 \end{bmatrix} + \left(\frac{x_2-x_1}{y_2-y_1} \right) \frac{1}{6} \begin{bmatrix} 2 & 1 & -1 & -2 \\ 1 & 2 & -2 & -1 \\ -1 & -2 & 2 & 1 \\ -2 & -1 & 1 & 2 \end{bmatrix}, \end{aligned} \quad (2.24)$$

Summing up all contributions from the related rectangular elements, we derive the global stiffness matrix and use the Gaussian quadrature to solve the linear system (2.19).

2.1.3 Features of CGFEMs

CGFEMs have fewer unknowns compared with MFEMs and WGFEMs. But the CGFEMs lack “local mass conservation” and “continuity of bulk normal fluxes”, which are two important physical properties of fluids such as water and oil [9, 27].

For example, we use CGP1 to show that CGFEMs don’t satisfy those two properties.

For simplicity, let

$$K = \begin{bmatrix} 1 & 0 \\ 0 & 1 \end{bmatrix},$$

so

$$f = \nabla \cdot (-\nabla p).$$

p_h is the numerical pressure and $\mathbf{u}_h = -\nabla p_h$ is the numerical velocity. Because ∇p_h is a constant vector on each element, the Darcy velocity \mathbf{u}_h is a constant vector on each element and $\nabla \cdot \mathbf{u}_h = 0$. On the local element T , by Gauss Divergence Theorem,

$$\int_{T^\partial} \mathbf{u}_h \cdot \mathbf{n} = \int_T \nabla \cdot \mathbf{u}_h = 0. \quad (2.25)$$

But $\int_T f$ is not necessarily to be 0. Therefore, CGFEMs don’t satisfy “local mass conservation”.

CGFEMs also lack “continuity of bulk normal fluxes”. Let γ be the interior edge shared by two adjacent elements. The values of bulk normal fluxes crossing γ of these two elements are different. In other words,

$$\int_\gamma \mathbf{u}_h|_{E_1} \cdot \mathbf{n}_1 + \int_\gamma \mathbf{u}_h|_{E_2} \cdot \mathbf{n}_2 \neq 0. \quad (2.26)$$

2.2.1 Mixed Formulation

MFEMs solve for the pressure and the Darcy velocity simultaneously. The Darcy equation is

$$\begin{cases} \nabla \cdot (-\mathbf{K}\nabla p) = f, & \text{in } \Omega, \\ p = p_D, & \text{on } \Gamma^D, \\ (-\mathbf{K}\nabla p) \cdot \mathbf{n} = u_N, & \text{on } \Gamma^N. \end{cases} \quad (2.27)$$

We introduce $\mathbf{u} = -(\mathbf{K}\nabla p)$, so the second order PDE system can be rewritten as the first order PDE system

$$\begin{cases} \mathbf{K}^{-1}\mathbf{u} + \nabla p = 0, & \text{in } \Omega, \\ \nabla \cdot \mathbf{u} = f, & \text{in } \Omega, \end{cases} \quad (2.28)$$

then multiply by test functions for each PDE.

In order to understand MFEMs well, we introduce spaces

$$\mathbf{H}(\text{div}; \Omega) = \{\mathbf{v} \in L^2(\Omega)^2 : \nabla \cdot \mathbf{v} \in L^2(\Omega)\}, \quad (2.29)$$

$$\mathbf{H}_{0,N}(\text{div}; \Omega) = \{\mathbf{v} \in \mathbf{H}(\text{div}; \Omega) : \mathbf{v} \cdot \mathbf{n} = 0 \text{ on } \Gamma^N\}, \quad (2.30)$$

$$\mathbf{H}_{u_N,N}(\text{div}; \Omega) = \{\mathbf{v} \in \mathbf{H}(\text{div}; \Omega) : \mathbf{v} \cdot \mathbf{n} = u_N \text{ on } \Gamma^N\}. \quad (2.31)$$

The mixed variational form for (2.28) is: Seek $\mathbf{u} \in \mathbf{H}_{u_N,N}(\text{div}, \Omega)$ and $p \in L^2(\Omega)$ such that

$$\begin{cases} \int_{\Omega} (\mathbf{K}^{-1}\mathbf{u}) \cdot \mathbf{v} - \int_{\Omega} p(\nabla \cdot \mathbf{v}) = - \int_{\Gamma^D} p_D \mathbf{v} \cdot \mathbf{n} - \int_{\Gamma^N} p(\mathbf{v} \cdot \mathbf{n}), & \forall \mathbf{v} \in \mathbf{H}_{0,N}(\text{div}; \Omega), \\ - \int_{\Omega} (\nabla \cdot \mathbf{u})q = - \int_{\Omega} fq, & \forall q \in L^2(\Omega), \end{cases} \quad (2.32)$$

because $\forall \mathbf{v} \in \mathbf{H}_{0,N}(\text{div}; \Omega)$, so $\mathbf{v} \cdot \mathbf{n} = 0$ on Γ^N , see Equation (2.30). The mixed variational

form becomes

$$\begin{cases} \int_{\Omega} (\mathbf{K}^{-1} \mathbf{u}) \cdot \mathbf{v} - \int_{\Omega} p(\nabla \cdot \mathbf{v}) = - \int_{\Gamma^D} p_D \mathbf{v} \cdot \mathbf{n}, & \forall \mathbf{v} \in \mathbf{H}_{0,N}(\text{div}; \Omega), \\ - \int_{\Omega} (\nabla \cdot \mathbf{u}) q = - \int_{\Omega} f q, & \forall q \in L^2(\Omega). \end{cases} \quad (2.33)$$

We introduce finite dimensional spaces

$$\begin{aligned} U_h &\subset H(\text{div}; \Omega); & U_h^N &\subset H_{u_N,N}(\text{div}; \Omega); & U_h^0 &\subset H_{0,N}(\text{div}; \Omega); \\ W_h &= \{q \in L^2(\Omega), q|_T = \text{constant}, \forall T \subset \mathcal{E}_h\}; \end{aligned} \quad (2.34)$$

$$\bar{U}_h = U_N + U_h, U_N \text{ is Neumann boundary conditions}; \quad \bar{U}_h^0 = U_h^0 + U_h.$$

MFEMs use pairs of finite element spaces, such as (RT_0, P_0) on triangles and $(RT_{[0]}, Q_0)$ on rectangles.

Mixed finite element scheme is formulated as: seek $\mathbf{u}_h \in \bar{U}_h$, $p_h \in W_h$ such that

$$\begin{cases} \sum_{E \in \mathcal{E}_h} \int_E (\mathbf{K}^{-1} \mathbf{u}_h) \cdot \mathbf{v} - \sum_{E \in \mathcal{E}_h} \int_E p_h (\nabla \cdot \mathbf{v}) = - \sum_{\gamma \in \Gamma_h^D} \int_{\gamma} p_D \mathbf{v} \cdot \mathbf{n}, & \forall \mathbf{v} \in U_h^0, \\ - \sum_{E \in \mathcal{E}_h} \int_E (\nabla \cdot \mathbf{u}_h) q = - \sum_{E \in \mathcal{E}_h} \int_E f q, & \forall q \in W_h. \end{cases} \quad (2.35)$$

MFEMs need to satisfy the inf-sup condition [21]. On a pair of mixed finite elements (\bar{U}_h, W_h) , the inf-sup condition is

$$\inf_{w \in \bar{W}_h, w \neq 0} \sup_{\mathbf{v} \in \bar{V}_h, \mathbf{v} \neq 0} \frac{(\nabla \cdot \mathbf{v}, w)}{\|\mathbf{v}\|_{H(\text{div})} \|w\|_{L^2}} > 0. \quad (2.36)$$

2.2.2 Raviart-Thomas Elements (RT_0, P_0) on Triangles

In MFEMs, we introduce pairs of finite element spaces for solving the velocity and pressure simultaneously. We will use basis functions in the Raviart-Thomas (RT) spaces to approximate the numerical velocity. Here, we discuss some basis functions in finite element

spaces [22, 3, 6, 13, 15, 21, 30, 31].

$$RT_K(T) = \mathcal{P}_K^d(T) + \mathbf{x}\mathcal{P}_K(T), \quad d = 2, \quad (2.37)$$

where \mathcal{P}_K is a \mathcal{P} -type polynomial, \mathbf{x} is a vector, T is a triangle. We use $RT_0(T)$ as an example.

Natural basis When $K = 0, d = 2$,

$$RT_0(T) = \text{Span} \left\{ \begin{bmatrix} 1 \\ 0 \end{bmatrix}, \begin{bmatrix} 0 \\ 1 \end{bmatrix}, \begin{bmatrix} x \\ y \end{bmatrix} \right\}. \quad (2.38)$$

Normalized basis

$$RT_0(T) = \text{Span} \left\{ \begin{bmatrix} 1 \\ 0 \end{bmatrix}, \begin{bmatrix} 0 \\ 1 \end{bmatrix}, \begin{bmatrix} X \\ Y \end{bmatrix} \right\}, \quad (2.39)$$

where $X = x - x_c, Y = y - y_c, (x_c, y_c)$ is the barycenter of T .

Edge-based basis

$$RT_0(T) = \text{Span} \{ \phi_1, \phi_2, \phi_3 \}, \quad (2.40)$$

and

$$\phi_1 = \frac{|e_1|}{2|T|}(P - P_1), \quad \phi_2 = \frac{|e_2|}{2|T|}(P - P_2), \quad \phi_3 = \frac{|e_3|}{2|T|}(P - P_3), \quad (2.41)$$

where $|e_i|$ is the length of the corresponding edge, $|T|$ is the area of the element, $P_i = (x_i, y_i)$ is the vertex of the triangle, $P = (x, y)$ is a moving point in the triangle, shown in Figure (2.4). There are two properties of edge-based basis functions in the RT space,

- $\phi_i \cdot n_j = \delta_{ij}$,
- $\nabla \cdot \phi_i = \frac{|e_i|}{|T|}$.

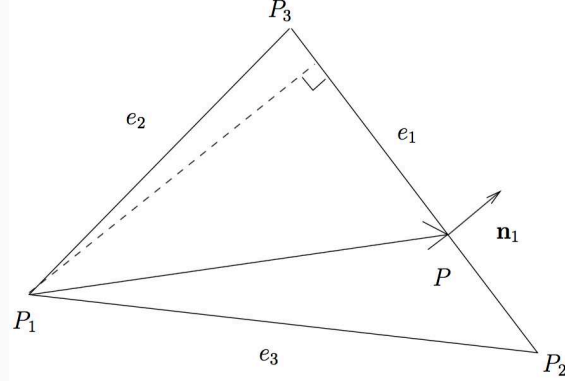


Figure 2.4: Edge-based basis for MFEMs

At the discrete level of triangular elements, we have

$RT_0(T)$: Local Raviart-Thomas space on each element T ,

$RT_0(\mathcal{T}_h)$: Global Raviart-Thomas space on the mesh \mathcal{T}_h .

And $RT_0(\mathcal{T}_h)$ is defined as

$$RT_0(\mathcal{T}_h) = \begin{cases} \mathbf{v} : \mathbf{v}|_E \in RT_0(T), \forall T \in \mathcal{T}_h; \\ \mathbf{v} \cdot \mathbf{n} \text{ is continuous across any interior of the mesh;} \\ \mathbf{v} \cdot \mathbf{n} = 0 \text{ on any boundary edge.} \end{cases}$$

We will use the global Raviart-Thomas space to approximate the velocity.

Implementation We show how to solve the Darcy equation on triangular meshes by MFEMs. In a pair of space, $\Phi_i (i = 1, 2, \dots, m)$ are the basis functions of RT_0 , $\Psi_i (i = 1, 2, \dots, n)$ are the basis functions defined on elements. So $\mathbf{u}_h = \sum_{i=1}^m c_i \Phi_i$, $p_h = \sum_{i=1}^n b_i \Psi_i$.

Then on each element T , we have

$$\begin{cases} \int_T (c_i \mathbf{K}^{-1} \Phi_i) \cdot \Phi_j - \int_T b_i \Psi_i (\nabla \cdot \Phi_j) = - \int_{\gamma} p_D \Phi_j \cdot \mathbf{n}, \\ \int_T c_i (\nabla \cdot \Phi_i) \Psi_j = - \int_T f \Psi_j. \end{cases} \quad (2.42)$$

In order to get the global matrix of the whole mesh, we calculate the local matrices and then assemble local ones into the global matrix.

On each element T , local edge-based basis functions, ϕ_1, ϕ_2, ϕ_3 , are defined in (2.41), and $\psi_i = 1$ on the very element. Then

$$\int_T \mathbf{K}^{-1} \phi_i \phi_j = \frac{1}{48|T|} \begin{bmatrix} \sigma_1 |e_1| & 0 & 0 \\ 0 & \sigma_2 |e_2| & 0 \\ 0 & 0 & \sigma_3 |e_3| \end{bmatrix} B^T (A \otimes \mathbf{K}^{-1}) B \begin{bmatrix} \sigma_1 |e_1| & 0 & 0 \\ 0 & \sigma_2 |e_2| & 0 \\ 0 & 0 & \sigma_3 |e_3| \end{bmatrix}, \quad (2.43)$$

and

$$\int_T (\nabla \cdot \phi_i) \psi_j = \sigma_i |e_i|. \quad (2.44)$$

The local matrices for calculating the above equations are

$$A = \begin{bmatrix} 2 & 1 & 1 \\ 1 & 2 & 1 \\ 1 & 1 & 2 \end{bmatrix}, \quad B = \begin{bmatrix} P_1 - P_1 & P_1 - P_2 & P_1 - P_3 \\ P_2 - P_1 & P_2 - P_2 & P_2 - P_3 \\ P_3 - P_1 & P_3 - P_2 & P_3 - P_3 \end{bmatrix}, \quad (2.45)$$

where P_1, P_2, P_3 are three vertices of a triangle, $|T|$ is the area of an element, σ_i is the sign function ensures the continuity of $(\mathbf{v} \cdot \mathbf{n})$ on edges, $|e_i|$ is the length of each edge. Matrix C^T is 3×3 , B^T is a 6×6 matrix, $(A \otimes \mathbf{K}^{-1})$ is 6×6 .

The finite element scheme on the whole mesh \mathcal{T}_h is formulated as

$$\begin{cases} \sum_{T \in \mathcal{T}_h} \int_T (c_i \mathbf{K}^{-1} \phi_i) \cdot \phi_j - \sum_{T \in \mathcal{T}_h} \int_T b_i \psi_i (\nabla \cdot \phi_j) = - \sum_{\gamma \in \Gamma_h^D} \int_{\gamma} p_D \phi_j \cdot \mathbf{n}, \\ - \sum_{T \in \mathcal{T}_h} \int_T c_i (\nabla \cdot \phi_i) \psi_j = - \sum_{T \in \mathcal{T}_h} \int_T f \psi_j, \end{cases} \quad (2.46)$$

where ϕ_i and ψ_i are local basis functions on each element. Use the former local matrices to assemble the global matrix.

2.2.3 Raviart-Thomas Element ($RT_{[0]}, Q_0$) on Rectangles

$$RT_{[K]}(E) = \mathcal{P}_{K+1,K} \times \mathcal{P}_{K,K+1}, \quad d = 2, \quad (2.47)$$

it is the cartesian product of $\mathcal{P}_{K+1,K}$ and $\mathcal{P}_{K,K+1}$, and $\mathcal{P}_{K+1,K} = \sum_{i=0}^{K+1} \sum_{j=0}^K a_{ij} x^i y^j$. For example, on a rectangle element E , when $K = 0, d = 2$, the natural basis is

$$RT_{[0]}(E) = \text{Span} \left\{ \begin{bmatrix} 1 \\ 0 \end{bmatrix}, \begin{bmatrix} 0 \\ 1 \end{bmatrix}, \begin{bmatrix} x \\ 0 \end{bmatrix}, \begin{bmatrix} 0 \\ y \end{bmatrix} \right\}. \quad (2.48)$$

At the discrete level, we have

$RT_{[0]}(E)$: Local Raviart-Thomas space on each element E ,

$RT_{[0]}(\mathcal{E}_h)$: Global Raviart-Thomas space on the mesh \mathcal{E}_h .

And $RT_{[0]}(\mathcal{E}_h)$ is defined as

$$RT_{[0]}(\mathcal{E}_h) = \begin{cases} \mathbf{v} : \mathbf{v}|_E \in RT_{[0]}(E), \forall E \in \mathcal{E}_h; \\ \mathbf{v} \cdot \mathbf{n} \text{ is continuous across any interior of the mesh;} \\ \mathbf{v} \cdot \mathbf{n} = 0 \text{ on any boundary edge.} \end{cases}$$

Implementations of MFEMs on rectangles are similar to MFEMs on triangles.

2.2.4 Features of MFEMs

Solutions have the properties “local mass conservation” and “bulk normal flux continuity”. We prove them on a rectangular mesh. The proof in a triangular mesh is identical.

“Local mass conservation” comes from the mixed variational form (2.33). Because $q \in L^2(\Omega)$, $q = 1$ on the element of the whole domain and $q = 0$ on the other edges and elements,

so we simplify the original mixed variational form as

$$-\int_E (\nabla \cdot \mathbf{u}) = -\int_E f. \quad (2.49)$$

Then by Gauss Divergence Theorem, we derive

$$-\int_{E^\partial} \mathbf{u} \cdot \mathbf{n} = -\int_E f. \quad (2.50)$$

This is “local mass conservation”.

As for “bulk normal flux continuity” on the rectangular element E , because $\mathbf{u} \in RT_{[0]}$, the space ensures the “bulk normal flux continuity”.

The disadvantage of MFEMs is that it results in indefinite discrete linear systems.

CHAPTER 3

WGFEMS FOR DARCY ON TWO-DIMENSIONAL MESHES

In this chapter, we introduce a family of relatively new finite element methods, called weak Galerkin finite element methods (WGFEMs) [20, 26, 25, 28]. WGFEMs use discrete weak functions to approximate the pressure and discrete weak gradients to approximate classical gradients.

To understand WGFEMs, we need to introduce some spaces. At the continuous level, we have spaces

- $L^2(\Omega)$: scalar functions;
- $H^1(\Omega)$: scalar functions;
- $L^2(\Omega)^2$: vector functions;
- $H(\text{div}, \Omega)$: vector functions, e.g., Darcy velocity.

Weak functions are defined as distributions [16]. The space of weak functions on an element E is defined as

$$W(E) := \{v = \{v^\circ, v^\partial\}, v^\circ \in L^2(E), v^\partial \in L^2(E^\partial)\}, \quad (3.1)$$

where v° is the value of v in the interior of E , v^∂ is the value of v on the boundary of E .

For a weak function v , its weak gradient $\nabla_w v$ is a functional defined through integration by parts,

$$(\nabla_w v, \mathbf{w}) = \int_{E^\partial} v^\partial(\mathbf{w} \cdot \mathbf{n}) - \int_E v^\circ(\nabla \cdot \mathbf{w}), \quad \forall \mathbf{w} \in H(\text{div}, E). \quad (3.2)$$

Suppose l, m are two non-negative integers. A discrete weak function space on the element E is

$$W(E, l, m) = \{v = \{v^\circ, v^\partial\}, v^\circ \in P^l(E^\circ), v^\partial \in P^m(E^\partial)\}, \quad (3.3)$$

where v° is a polynomial with degree $\leq l$ defined in E° , v^∂ is a polynomial with degree $\leq m$ defined on E^∂ .

Let \mathcal{E}_h be a collection of elements. Two spaces of discrete weak functions on the mesh \mathcal{E}_h are

$$S_h(l, m) = \{v = \{v^\circ, v^\partial\} : v|_E \in W(E, l, m), \forall E \in \mathcal{E}_h\}, \quad (3.4)$$

$$S_h^0(l, m) = \{v = \{v^\circ, v^\partial\} \in S_h(l, m) : v^\partial|_{E^\partial \cap \Gamma^D} = 0, \forall E \in \mathcal{E}_h\}, \quad (3.5)$$

where Γ^D represents Dirichlet boundaries.

For a discrete weak function, its discrete weak gradient $\nabla_{w,d}v$ is a functional defined on $P^n(E)^2$ via integration by parts,

$$\int_E (\nabla_{w,d}v) \cdot \mathbf{w} = \int_{E^\partial} v^\partial(\mathbf{w} \cdot \mathbf{n}) - \int_{E^\circ} v^\circ(\nabla \cdot \mathbf{w}), \quad \forall \mathbf{w} \in P^n(E)^2, \quad (3.6)$$

where n is a non-negative integer.

In CGFEMs, the shape functions are continuous polynomials. But in WGFEMs, we use discrete weak functions as shape functions. Generally, the discrete weak function $v^\circ \in P^l(E^\circ)$, $v^\partial \in P^m(E^\partial)$, and the discrete weak gradient $\nabla_{w,d}v \in P^n(E)^2$. We will consider triangular, rectangular and quadrilateral elements E .

For example, if E is a triangular element, the spaces of WGFEMs could be chosen as $(P_0, P_0; RT_0)$, and $RT_0 \subset P^1(E)^2$, where

$$P^1(E)^2 = \begin{bmatrix} a_0 + a_1x + a_2y \\ b_0 + b_1x + b_2y \end{bmatrix}. \quad (3.7)$$

With this choice, $l = 0, m = 0, n = 1$. Additionally, we can also choose $(P_1, P_1; RT_1)$, and

$RT_1 \subset P^2(E)^2$, where

$$RT_1 = \left\{ \begin{bmatrix} 1 \\ 0 \end{bmatrix}, \begin{bmatrix} x \\ 0 \end{bmatrix}, \begin{bmatrix} y \\ 0 \end{bmatrix}, \begin{bmatrix} 0 \\ 1 \end{bmatrix}, \begin{bmatrix} 0 \\ x \end{bmatrix}, \begin{bmatrix} 0 \\ y \end{bmatrix}, \begin{bmatrix} x^2 \\ xy \end{bmatrix}, \begin{bmatrix} xy \\ y^2 \end{bmatrix} \right\}, \quad (3.8)$$

$$P^2(E)^2 = \left\{ \begin{array}{l} a_0 + a_1x + a_2x^2 + a_3y + a_4y^2 + a_5xy \\ b_0 + b_1x + b_2x^2 + b_3y + b_4y^2 + b_5xy \end{array} \right\}. \quad (3.9)$$

In this case, $l = 1, m = 1, n = 2$.

If E is a rectangular element, $WG(Q_0, Q_0; RT_{[0]})$ could be selected. $RT_{[0]}$ is defined in Chapter 2. So in this case, $l = 0, m = 0, n = 1$. In the following sections, we will further discuss weak Galerkin finite elements on quadrilaterals.

In MFEMs, we used the global Raviart-Thomas space to approximate the numerical velocity, see Section 2.2.2. In WGFEMs, we will use the broken Raviart-Thomas space, $\Pi_{T \in \mathcal{T}_h} RT_0(T)$, to approximate discrete weak gradients on triangles. The global Raviart-Thomas space is the subspace of the broken Raviart-Thomas space. So our solutions are in a bigger space. We will prove bulk normal flux continuity by WGFEMs.

3.1 LOWEST ORDER WG FINITE ELEMENTS ON TRIANGLES AND QUADRILATERALS

In this section, we will discuss WGFEMs on triangles and quadrilaterals. Rectangles are regarded as a special case of quadrilaterals [2, 4, 5, 11].

3.1.1 Triangular Elements

RT_0 on Triangles

On each triangular element with vertices $(x_i, y_i), i = 1, 2, 3$, the local Raviart-Thomas space $RT_0 = \text{Span}(\mathbf{w}_1, \mathbf{w}_2, \mathbf{w}_3)$, with $\mathbf{w}_1 = \begin{bmatrix} 1 \\ 0 \end{bmatrix}$, $\mathbf{w}_2 = \begin{bmatrix} 0 \\ 1 \end{bmatrix}$, $\mathbf{w}_3 = \begin{bmatrix} X \\ Y \end{bmatrix}$. The Gram

matrix of the basis functions is

$$GM = \begin{bmatrix} (\mathbf{w}_1, \mathbf{w}_1) & (\mathbf{w}_1, \mathbf{w}_2) & (\mathbf{w}_1, \mathbf{w}_3) \\ (\mathbf{w}_2, \mathbf{w}_1) & (\mathbf{w}_2, \mathbf{w}_2) & (\mathbf{w}_2, \mathbf{w}_3) \\ (\mathbf{w}_3, \mathbf{w}_1) & (\mathbf{w}_3, \mathbf{w}_2) & (\mathbf{w}_3, \mathbf{w}_3) \end{bmatrix} = \begin{bmatrix} |T| & 0 & 0 \\ 0 & |T| & 0 \\ 0 & 0 & S \end{bmatrix}, \quad (3.10)$$

where $|T|$ is the area of an triangle element, and

$$S = \frac{|T|}{36} ((x_1 - x_2)^2 + (x_2 - x_3)^2 + (x_3 - x_1)^2 + (y_1 - y_2)^2 + (y_2 - y_3)^2 + (y_3 - y_1)^2).$$

WG($P_0, P_0; RT_0$) Elements on Triangles

WG($P_0, P_0; RT_0$) means that all discrete weak functions are degree 0 polynomials and discrete weak gradients are defined in RT_0 space. We use discrete weak functions to approximate the pressure in interiors and on the boundaries of the element T .

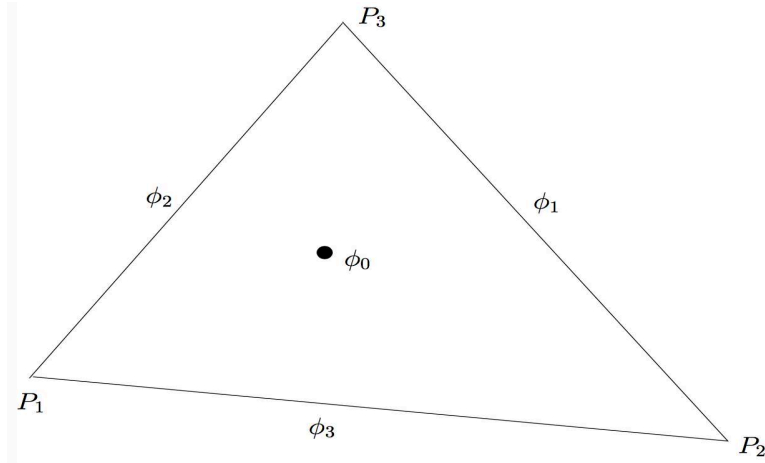


Figure 3.1: Weak functions on a triangle

On each triangular element, there are four weak functions: $\phi_0, \phi_1, \phi_2, \phi_3$, as shown in Figure (3.1):

- $\phi_0 = 1$ in the interior, $\phi_0 = 0$ on the three edges;

- $\phi_i = 1$ ($i = 1, 2, 3$) on the very edge, $\phi_i = 0$ on the other edges and in the interior.

The discrete weak gradient $\nabla_{w,d}\phi$ is specified in the Raviart-Thomas space. By definition of the discrete weak gradient, we have

$$\int_T (\nabla_{w,d}\phi) \cdot \mathbf{w} = \int_{T^\partial} \phi^\partial(\mathbf{w} \cdot \mathbf{n}) - \int_{T^\circ} \phi^\circ(\nabla \cdot \mathbf{w}), \quad \forall \mathbf{w} \in RT_0(T). \quad (3.11)$$

Let $\nabla_{w,d}\phi = \sum_{i=1}^3 c_i \mathbf{w}_i$, where \mathbf{w}_i are defined above.

On each local element, we have

$$\sum_{i=1}^3 c_i \int_T \mathbf{w}_i \cdot \mathbf{w}_j = \int_{T^\partial} \phi^\partial(\mathbf{w}_j \cdot \mathbf{n}) - \int_{T^\circ} \phi^\circ(\nabla \cdot \mathbf{w}_j). \quad (3.12)$$

Since $\phi_0^\circ = 1, \phi_0^\partial = 0$ and $\phi_i^\partial = 1, \phi_i^\circ = 0$ ($i = 1, 2, 3$), we can simplify Equation (3.12).

For example, on an element T , $\nabla_{w,d}\phi_0 = \sum_{i=1}^3 c_i \mathbf{w}_i$. And it is easy to see that $\nabla \cdot \mathbf{w}_1 = 0, \nabla \cdot \mathbf{w}_2 = 0, \nabla \cdot \mathbf{w}_3 = 2$. Since $\phi_0^\circ = 1, \phi_0^\partial = 0$,

$$\int_{T^\partial} \phi_0^\partial(\mathbf{w} \cdot \mathbf{n}) = 0.$$

Then (3.12) for ϕ_0 becomes

$$\sum_{i=1}^3 c_i \int_T \mathbf{w}_i \cdot \mathbf{w}_j = - \int_{T^\circ} \phi_0^\circ(\nabla \cdot \mathbf{w}_j), \quad (3.13)$$

Using (3.10), we solve for the coefficients and

$$\nabla_{w,d}\phi_0 = 0\mathbf{w}_1 + 0\mathbf{w}_2 + \frac{-2|T|}{S}\mathbf{w}_3. \quad (3.14)$$

As for the coefficients of $\nabla_{w,d}\phi_1$, since $\phi_1^{e_1} = 1$ on the first edge, $\phi_1^\partial = 0$ on the other edges, $\phi_1^\circ = 0$, so

$$- \int_{T^\circ} \phi_1^\circ(\nabla \cdot \mathbf{w}_j) = 0.$$

Then (3.12) for ϕ_1 becomes

$$\sum_{i=1}^3 c_i \int_T \mathbf{w}_i \cdot \mathbf{w}_j = \int_{e_1} \phi_1^{e_1}(\mathbf{w}_j \cdot \mathbf{n}_1) = \int_{e_1} (\mathbf{w}_j \cdot \mathbf{n}_1). \quad (3.15)$$

Using (3.10), we solve for the coefficients and

$$\nabla_{w,d}\phi_1 = \frac{(y_3 - y_2)}{|T|} \mathbf{w}_1 + \frac{(x_2 - x_3)}{|T|} \mathbf{w}_2 + \frac{2|T|}{3S} \mathbf{w}_3. \quad (3.16)$$

In the end, we have

$$\left\{ \begin{array}{l} \nabla_{w,d}\phi_0 = 0\mathbf{w}_1 + 0\mathbf{w}_2 + \frac{-2|T|}{S} \mathbf{w}_3, \\ \nabla_{w,d}\phi_1 = \frac{(y_3 - y_2)}{|T|} \mathbf{w}_1 + \frac{(x_2 - x_3)}{|T|} \mathbf{w}_2 + \frac{2|T|}{3S} \mathbf{w}_3, \\ \nabla_{w,d}\phi_2 = \frac{(y_1 - y_3)}{|T|} \mathbf{w}_1 + \frac{(x_3 - x_1)}{|T|} \mathbf{w}_2 + \frac{2|T|}{3S} \mathbf{w}_3, \\ \nabla_{w,d}\phi_3 = \frac{(y_2 - y_1)}{|T|} \mathbf{w}_1 + \frac{(x_1 - x_2)}{|T|} \mathbf{w}_2 + \frac{2|T|}{3S} \mathbf{w}_3. \end{array} \right. \quad (3.17)$$

It is used to calculate the global stiffness matrix of the WG finite element scheme on a triangular mesh.

3.1.2 Quadrilateral Elements

$RT_{[0]}$ on Quadrilaterals

On each quadrilateral element, the local Raviart-Thomas space

$$RT_{[0]} = \text{Span}(\mathbf{w}_1, \mathbf{w}_2, \mathbf{w}_3, \mathbf{w}_4), \quad (3.18)$$

with $\mathbf{w}_1 = \begin{bmatrix} 1 \\ 0 \end{bmatrix}$, $\mathbf{w}_2 = \begin{bmatrix} 0 \\ 1 \end{bmatrix}$, $\mathbf{w}_3 = \begin{bmatrix} X \\ 0 \end{bmatrix}$, $\mathbf{w}_4 = \begin{bmatrix} 0 \\ Y \end{bmatrix}$. The Gram matrix of basis functions is

$$GM = \begin{bmatrix} (\mathbf{w}_1, \mathbf{w}_1) & (\mathbf{w}_1, \mathbf{w}_2) & (\mathbf{w}_1, \mathbf{w}_3) & (\mathbf{w}_1, \mathbf{w}_4) \\ (\mathbf{w}_2, \mathbf{w}_1) & (\mathbf{w}_2, \mathbf{w}_2) & (\mathbf{w}_2, \mathbf{w}_3) & (\mathbf{w}_2, \mathbf{w}_4) \\ (\mathbf{w}_3, \mathbf{w}_1) & (\mathbf{w}_3, \mathbf{w}_2) & (\mathbf{w}_3, \mathbf{w}_3) & (\mathbf{w}_3, \mathbf{w}_4) \\ (\mathbf{w}_4, \mathbf{w}_1) & (\mathbf{w}_4, \mathbf{w}_2) & (\mathbf{w}_4, \mathbf{w}_3) & (\mathbf{w}_4, \mathbf{w}_4) \end{bmatrix} = \begin{bmatrix} |E| & 0 & \int_E X & 0 \\ 0 & |E| & 0 & \int_E Y \\ \int_E X & 0 & \int_E X^2 & 0 \\ 0 & \int_E Y & 0 & \int_E Y^2 \end{bmatrix}. \quad (3.19)$$

where $|E|$ is the area of the quadrilateral element. When E is a rectangle as a special case, the Gram matrix becomes a diagonal matrix with $\int_E X$ and $\int_E Y = 0$.

WG($Q_0, Q_0; RT_{[0]}$) Elements on Quadrilaterals

WG($Q_0, Q_0; RT_{[0]}$) means that all of discrete weak functions are degree 0 polynomials and discrete weak gradients are in $RT_{[0]}$ space. Discrete weak functions are defined in interiors and on the boundaries of an element E . On each quadrilateral element, there are five weak

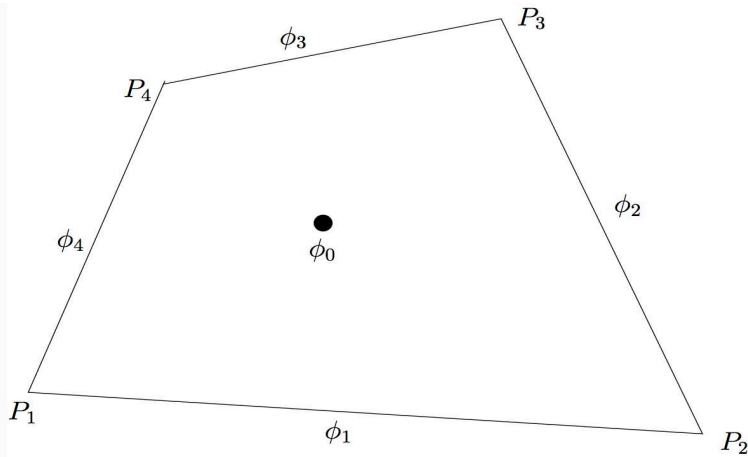


Figure 3.2: Weak functions on a quadrilateral

functions: $\phi_0, \phi_1, \phi_2, \phi_3, \phi_4$, as shown in Figure (3.2):

- $\phi_0 = 1$ in the interior, $\phi_0 = 0$ on the four edges;

- $\phi_i = 1$ ($i = 1, 2, 3, 4$) on the very edge, $\phi_i = 0$ on the other edges and in the interior.

The discrete weak gradient $\nabla_{w,d}\phi$ is specified in the Raviart-Thomas space, so $\nabla_{w,d}\phi = \sum_{i=1}^4 c_i \mathbf{w}_i$. Through integration by parts [28], we have a small linear system,

$$\int_E (\nabla_{w,d}\phi) \cdot \mathbf{w} = \int_{E^\partial} \phi^\partial (\mathbf{w} \cdot \mathbf{n}) - \int_{E^\circ} \phi^\circ (\nabla \cdot \mathbf{w}), \quad \forall \mathbf{w} \in RT_{[0]}(E). \quad (3.20)$$

On each local element, we have

$$\sum_{i=1}^4 c_i \int_E \mathbf{w}_i \cdot \mathbf{w}_j = \int_{E^\partial} \phi^\partial (\mathbf{w}_j \cdot \mathbf{n}) - \int_{E^\circ} \phi^\circ (\nabla \cdot \mathbf{w}_j), \quad (3.21)$$

the left hand side is a multiplication of coefficients and the Gram matrix. Since we define $\phi_0^\circ = 1, \phi_0^\partial = 0, \phi_i^\partial = 1, \phi_i^\circ = 0, (i = 1, 2, 3, 4)$, we can simplify the right hand side when we do calculations. The computations are similar to what we have discussed for coefficients on triangles.

When E is a rectangle as a special case, we derive the following equations

$$\left\{ \begin{array}{l} \nabla_{w,d}\phi_0 = 0\mathbf{w}_1 + 0\mathbf{w}_2 + \frac{-12}{(x_2-x_1)^2}\mathbf{w}_3 + \frac{-12}{(y_2-y_1)^2}\mathbf{w}_4, \\ \nabla_{w,d}\phi_1 = 0\mathbf{w}_1 + \frac{-1}{y_2-y_1}\mathbf{w}_2 + 0\mathbf{w}_3 + \frac{6}{(y_2-y_1)^2}\mathbf{w}_4, \\ \nabla_{w,d}\phi_2 = \frac{1}{x_2-x_1}\mathbf{w}_1 + 0\mathbf{w}_2 + \frac{6}{(x_2-x_1)^2}\mathbf{w}_3 + 0\mathbf{w}_4, \\ \nabla_{w,d}\phi_3 = 0\mathbf{w}_1 + \frac{1}{y_2-y_1}\mathbf{w}_2 + 0\mathbf{w}_3 + \frac{6}{(y_2-y_1)^2}\mathbf{w}_4, \\ \nabla_{w,d}\phi_4 = \frac{-1}{x_2-x_1}\mathbf{w}_1 + 0\mathbf{w}_2 + \frac{6}{(x_2-x_1)^2}\mathbf{w}_3 + 0\mathbf{w}_4. \end{array} \right. \quad (3.22)$$

It is used to calculate the global stiffness matrix of the WG finite element scheme on a rectangular mesh.

3.2 WGFEMs FOR DARCY

For the Darcy equation, our unknown is the pressure p . We define pressure $p \in H^1(\Omega)$. After we calculate the pressure, we calculate the Darcy velocity \mathbf{u} .

Using WGFEMs for solving the Darcy equation, we define weak functions in weak finite element spaces, construct discrete weak gradients in the local Raviart-Thomas spaces.

The weak form of the Darcy equation derived via integration by parts is: seek $p \in H_{D,p_D}^1(\Omega)$, such that

$$\int_{\Omega} \mathbf{K} \nabla p \cdot \nabla q = \int_{\Omega} f q - \int_{\Gamma^N} u_N q, \quad q \in H_{D,0}^1(\Omega), \quad (3.23)$$

where $H_{D,p_D}^1(\Omega) = \{q \in H^1(\Omega) : q|_{\Gamma^D} = p_D\}$, $H_{D,0}^1(\Omega) = \{q \in H^1(\Omega) : q|_{\Gamma^D} = 0\}$.

Then the WG finite element scheme of the Darcy equation is, seek $p_h = \{p_h^{\circ}, p_h^{\partial}\} \in S_h$ such that $p_h^{\partial}|_{\Gamma_h^D} = \mathbf{Q}_h^{\partial}(p_D)$ (L^2 -projection of Dirichlet boundary data into the space of piecewise constants on Γ_h^D) and

$$\mathcal{A}_h(p_h, q) = \mathcal{F}(q), \quad \forall q = \{q^{\circ}, q^{\partial}\} \in S_h^0, \quad (3.24)$$

where

$$\mathcal{A}_h(p_h, q) := \sum_{E \in \mathcal{E}_h} \int_E \mathbf{K} \nabla_{w,d} p_h \cdot \nabla_{w,d} q, \quad (3.25)$$

and

$$\mathcal{F}(q) := \sum_{E \in \mathcal{E}_h} \int_E f q^{\circ} - \sum_{\gamma \in \Gamma_h^N} \int_{\gamma} u_N q^{\partial}. \quad (3.26)$$

We can solve for the numerical pressure p_h . The discrete weak gradient $\nabla_{w,d} p_h$ is calculated in each element. And $\nabla_{w,d} p_h$ is in the local RT space. So for the velocity $\mathbf{u}_h = -\mathbf{K} \nabla_{w,d} p_h$, we take the L_2 -projection \mathbf{Q}_h to project it into the local RT space. Finally, on an edge e of an element E , the flux $\int_e \mathbf{u}_h \cdot \mathbf{n}$ is calculated.

3.3 PROPERTIES AND CONVERGENCE

WGFEMs satisfy two important physical properties, which we will prove using WGFEMs on some arbitrary discretizations. We state a proposition about the convergence rates in pressure, velocity and flux.

3.3.1 Local Mass Conservation

Theorem: On each element of the mesh, with \mathbf{n} being the outward normal vector on the boundary, \mathbf{u}_h being the numerical velocity,

$$\int_{E^\partial} \mathbf{u}_h \cdot \mathbf{n} = \int_E f. \quad (3.27)$$

Proof.

Take a test function q so that $q|_{E^\circ} = 1$ but $q|_{E^\partial} = 0$. Use the definition of discrete weak gradient and Gauss Divergence Theorem, we have the following equations

$$\begin{aligned} \int_E f &= \int_E (\mathbf{K} \nabla_{w,d} p_h) \cdot \nabla_{w,d} q = \int_E \mathbf{Q}_h(\mathbf{K} \nabla_{w,d} p_h) \cdot \nabla_{w,d} q \\ &= - \int_E \mathbf{u}_h \cdot \nabla_{w,d} q = - \int_{E^\partial} q^\partial (\mathbf{u}_h \cdot \mathbf{n}) + \int_{E^\circ} q^\circ (\nabla \cdot \mathbf{u}_h) \\ &= \int_{E^\circ} \nabla \cdot \mathbf{u}_h = \int_{E^\partial} \mathbf{u}_h \cdot \mathbf{n}. \end{aligned}$$

The first equal sign comes from $\int_E f q^\circ = \int_E f$ because $q^\circ = 1$. \mathbf{Q}_h is the projection ensures $(\mathbf{K} \nabla_{w,d} p_h)$ in the finite element space. The third equal sign comes from the definition of \mathbf{u}_h , the fourth and fifth are the use of integration by parts and values of q . In the end, we use Gauss Divergence theorem and finish the proof.

3.3.2 Normal Flux Continuity

Theorem: An interior edge γ shared by two neighboring elements E_1, E_2 , with $\mathbf{n}_1, \mathbf{n}_2$ as outward normal vectors:

$$\int_{\gamma} \mathbf{u}_h|_{E_1} \cdot \mathbf{n}_1 + \int_{\gamma} \mathbf{u}_h|_{E_2} \cdot \mathbf{n}_2 = 0. \quad (3.28)$$

Proof.

We take a test function $q = \{q^\circ, q^\partial\}$, $q^\partial = 1$ only on the very edge γ , $q^\partial = 0$ on other edges and in interiors, $q^\circ = 0$ in interiors. Applying the projection \mathbf{Q}_h , and the definition of the discrete weak gradient, we have

$$\begin{aligned} 0 &= \int_{E_1} (\mathbf{K}\nabla_{w,d}p_h) \cdot \nabla_{w,d}q + \int_{E_2} (\mathbf{K}\nabla_{w,d}p_h) \cdot \nabla_{w,d}q \\ &= \int_{E_1} \mathbf{Q}_h(\mathbf{K}\nabla_{w,d}p_h) \cdot \nabla_{w,d}q + \int_{E_2} \mathbf{Q}_h(\mathbf{K}\nabla_{w,d}p_h) \cdot \nabla_{w,d}q \\ &= \int_{E_1} (-\mathbf{u}_h^{(1)}) \cdot \nabla_{w,d}q + \int_{E_2} (-\mathbf{u}_h^{(2)}) \cdot \nabla_{w,d}q \\ &= - \int_{\gamma} \mathbf{u}_h^{(1)} \cdot \mathbf{n}_1 q^\partial + \int_{E_1^\circ} \mathbf{u}_h^{(1)} q^\circ - \int_{\gamma} \mathbf{u}_h^{(2)} \cdot \mathbf{n}_2 q^\partial + \int_{E_2^\circ} \mathbf{u}_h^{(2)} q^\circ \\ &= - \int_{\gamma} \mathbf{u}_h^{(1)} \cdot \mathbf{n}_1 - \int_{\gamma} \mathbf{u}_h^{(2)} \cdot \mathbf{n}_2. \end{aligned}$$

The first equal sign comes from the WGFEMs scheme (3.24). Because we define $q^\partial = 1$ on γ , $q^\circ = 0$ in interiors, so $q^\partial = 0$ on the Neumann boundaries, so the value of right hand side of the WG scheme is 0. Since the discrete weak gradients have contributions from the two adjacent elements, then $\int_{E_1} (\mathbf{K}\nabla_{w,d}p_h) \cdot \nabla_{w,d}q + \int_{E_2} (\mathbf{K}\nabla_{w,d}p_h) \cdot \nabla_{w,d}q = 0$. The second equal sign is the use of projection to ensure $(\mathbf{K}\nabla_{w,d}p_h)$ is still in $RT_{[0]}$. The third one is the definition of \mathbf{u}_h , the next two equal signs are the use of integration by parts and how to define values of q .

In MFEMs, \mathbf{u}_h is in the global Raviart-Thomas space, which is the finite dimensional subspace of $H(\text{div})$. In WGFEMs, we enforce the discrete weak gradients to be in the RT

space and calculate \mathbf{u}_h . Actually, we can prove that the numerical Darcy velocity calculated by WGFEMs is in a subspace of $H(\text{div})$.

In Equation (3.28), $\mathbf{n}_1 = -\mathbf{n}_2$ on the interior edge γ . Let \mathbf{n}_E be the outward normal vector with respect to E_1 . We rewrite the equation to be

$$\int_{\gamma} (\mathbf{u}_h|_{E_1} - \mathbf{u}_h|_{E_2}) \cdot \mathbf{n}_E = \int_{\gamma} \mathbf{u}_h \cdot \mathbf{n}_E = 0. \quad (3.29)$$

Since components of \mathbf{u}_h and \mathbf{n}_E are constants on γ , we have $\mathbf{u}_h \cdot \mathbf{n}_E = 0$ on γ , which means that the normal component of \mathbf{u}_h is continuous across the edge γ . For the whole mesh \mathcal{E}_h , we can also see that $\mathbf{u}_h \cdot \mathbf{n}_E = 0$ on all interior edges. So the normal component of \mathbf{u}_h is continuous across all interior edges of the mesh. From the **Lemma 3.66** of [19], if $\mathbf{u}_h \cdot \mathbf{n}_E$ is continuous for all interior edges of the mesh, \mathbf{u}_h is in a subspace of $H(\text{div})$. So the numerical Darcy velocity is in the subspace of $H(\text{div})$.

3.3.3 Convergence

Proposition (Convergence in pressure, velocity, and flux) [24]. p is the exact solution of the Darcy problem and $\mathbf{u} = -\mathbf{K}\nabla p$. The exact solution has regularity $p \in H^{1+s}(\Omega)$ and $\mathbf{u} \in H^s(\Omega)^2$ for some $s \in (0, 1]$. When the quadrilaterals are asymptotically parallelograms, there hold

$$\|p - p_h^\circ\| \leq Ch, \quad \|\mathbf{u} - \mathbf{u}_h\| \leq Ch^s, \quad \|(\mathbf{u} - \mathbf{u}_h) \cdot \mathbf{n}\| \leq Ch^s, \quad (3.30)$$

where $C > 0$ is a constant that is independent of the mesh size h .

We will see the convergence rates of several examples in a later section.

To measure the errors in pressure, Darcy velocity and flux for WGFEMs, we use L^2 norms, which is defined as $\|f\|_{L^2(\Omega)} = (\int_{\Omega} |f|^2)^{\frac{1}{2}}$,

$$\|p - p_h^\circ\|^2 = \sum_{E \in \mathcal{E}_h} \|p - p_h^\circ\|_{L^2(E)}^2, \quad (3.31)$$

$$\|\mathbf{u} - \mathbf{u}_h\|^2 = \sum_{E \in \mathcal{E}_h} \|\mathbf{u} - \mathbf{u}_h\|_{L^2(E)}^2, \quad (3.32)$$

$$\|(\mathbf{u} - \mathbf{u}_h) \cdot \mathbf{n}\|^2 = \sum_{E \in \mathcal{E}_h} \sum_{\gamma \subset E^\partial} \frac{|E|}{|\gamma|} \|\mathbf{u} \cdot \mathbf{n} - \mathbf{u}_h \cdot \mathbf{n}\|_{L^2(\gamma)}^2. \quad (3.33)$$

3.4 LOWEST ORDER WG SCHEME FOR THE DARCY EQUATION

In this section, we will use $WG(Q_0, Q_0; RT_{[0]})$ to solve the Darcy equation [17, 23]. The WG scheme of the lowest order is the same as the general scheme we discussed in Section 3.2. The space for discrete weak functions is Q_0 , the space for discrete weak gradients is $RT_{[0]}$. Solving by $WG(P_0, P_0; RT_0)$ has the same idea as solving by $WG(Q_0, Q_0; RT_{[0]})$. The differences are in basis functions of the Raviart-Thomas spaces and weak functions of WGFEMs.

On the space of weak functions, S_h , we have weak functions defined in interiors and on edges. In the finite element space $RT_{[0]}$, discrete weak gradients are linear combinations of basis functions of $RT_{[0]}$, so we construct 5×5 local stiffness matrices and then assemble them to get the global stiffness matrix.

WG($Q_0, Q_0; RT_{[0]}$) Scheme for the Darcy Equation

Seek $p_h = \{p_h^\circ, p_h^\partial\} \in S_h$ such that $p_h^\partial|_{\Gamma_h^D} = \mathbf{Q}_h^\partial(p_D)$ (L^2 -projection of Dirichlet boundary data into the space of piecewise constants on Γ_h^D) and

$$\mathcal{A}_h(p_h, q) = \mathcal{F}(q), \quad \forall q = \{q^\circ, q^\partial\} \in S_h^0, \quad (3.34)$$

where

$$\mathcal{A}_h(p_h, q) := \sum_{E \in \mathcal{E}_h} \int_E \mathbf{K} \nabla_{w,d} p_h \cdot \nabla_{w,d} q, \quad (3.35)$$

and

$$\mathcal{F}(q) := \sum_{E \in \mathcal{E}_h} \int_E f q^\circ - \sum_{\gamma \in \Gamma_h^N} \int_\gamma u_N q^\partial. \quad (3.36)$$

The left hand side of the scheme is a multiplication of coefficients and the global stiffness matrix. Based on how we define ϕ_i , we can simplify the terms of right hand side to be

$$\begin{aligned} \sum_{E \in \mathcal{E}_h} \int_E f q^\circ &= \sum_{E \in \mathcal{E}_h} \int_E f, \\ \sum_{\gamma \in \Gamma_h^N} \int_\gamma u_N q^\partial &= \sum_{\gamma \in \Gamma_h^N} \int_\gamma u_N. \end{aligned}$$

Bilinear mapping When we perform calculations, such as calculating integrals on quadrilaterals, we use the bilinear mapping to map the unit square $[0, 1]^2$ onto a quadrilateral.

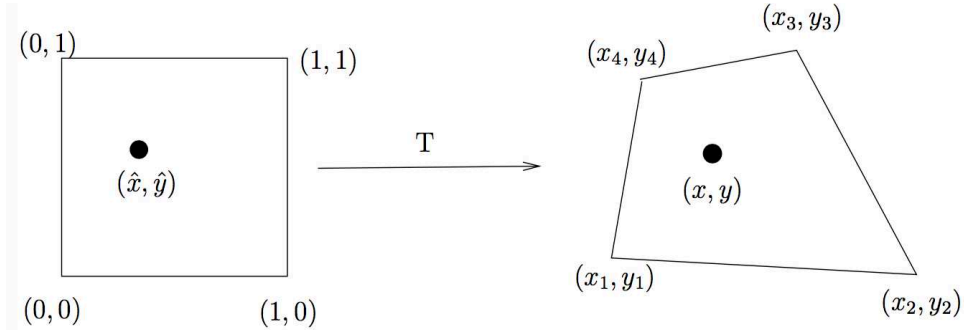


Figure 3.3: Mapping from the unit square to a quadrilateral.

The relation between coordinates on the unit square and on the quadrilateral is

$$\begin{cases} x = a_1 + a_2 \hat{x} + a_3 \hat{y} + a_4 \hat{x} \hat{y}, \\ y = b_1 + b_2 \hat{x} + b_3 \hat{y} + b_4 \hat{x} \hat{y}, \end{cases} \quad (3.37)$$

where

$$\begin{cases} a_1 = x_1 \\ b_1 = y_1 \end{cases} \begin{cases} a_2 = x_2 - x_1 \\ b_2 = y_2 - y_1 \end{cases} \begin{cases} a_3 = x_4 - x_1 \\ b_3 = y_4 - y_1 \end{cases} \begin{cases} a_4 = (x_1 + x_3) - (x_2 + x_4) \\ b_4 = (y_1 + y_3) - (y_2 + y_4) \end{cases} \quad (3.38)$$

and $(x_i, y_i)(i = 1, 2, 3, 4)$ are four vertices of the quadrilateral element and $(\hat{x}, \hat{y}) \in [0, 1]^2$. The Jacobian matrix used for calculating the mapping is

$$\mathbf{J} = \begin{bmatrix} \frac{\partial x}{\partial \hat{x}} & \frac{\partial x}{\partial \hat{y}} \\ \frac{\partial y}{\partial \hat{x}} & \frac{\partial y}{\partial \hat{y}} \end{bmatrix} = \begin{bmatrix} a_2 + a_4 \hat{y} & a_3 + a_4 \hat{x} \\ b_2 + b_4 \hat{y} & b_3 + b_4 \hat{x} \end{bmatrix}, \quad (3.39)$$

the Jacobian determinant is

$$\begin{aligned} J = \det(\mathbf{J}) &= (a_2 b_3 - a_3 b_2) + (a_2 b_4 - a_4 b_2) \hat{x} + (a_4 b_3 - a_3 b_4) \hat{y} \\ &= \begin{vmatrix} a_2 & a_3 \\ b_2 & b_3 \end{vmatrix} + \begin{vmatrix} a_2 & a_4 \\ b_2 & b_4 \end{vmatrix} \hat{x} + \begin{vmatrix} a_4 & a_3 \\ b_4 & b_3 \end{vmatrix} \hat{y}. \end{aligned} \quad (3.40)$$

The above results indicate that the Jacobian determinant is a linear polynomial of \hat{x}, \hat{y} . We will use this change of variables to calculate definite integrals on quadrilateral elements.

For example, if we calculate $\int_E f dE$ by the K-point Gaussian quadrature on a quadrilateral element E , then

$$\int_E f dE \approx \sum_{k=1}^K w_k f(x, y) J, \quad E \in \mathcal{E}_h, \quad (3.41)$$

where w_k is the weight, J is the determinant of Jacobian matrix.

Numerical pressure On a quadrilateral mesh \mathcal{E}_h ,

$$S_h(l, m) = \text{Span}\{\Phi_1, \Phi_2, \dots, \Phi_n, \Phi_{n+1}, \dots, \Phi_m\},$$

where $\Phi_1, \Phi_2, \dots, \Phi_n$, are defined in the interiors of all elements, n is the number of elements of the mesh, $\Phi_{n+1}, \dots, \Phi_m$ are defined on the edges of the mesh. Let $\phi_0, \phi_1, \phi_2, \phi_3, \phi_4$ be the basis functions on each quadrilateral element E .

The element stiffness matrix on each element is

$$\begin{bmatrix} \int_E \mathbf{K} \nabla_{w,d} \phi_0 \cdot \nabla_{w,d} \phi_0 & \int_E \mathbf{K} \nabla_{w,d} \phi_0 \cdot \nabla_{w,d} \phi_1 & \int_E \mathbf{K} \nabla_{w,d} \phi_0 \cdot \nabla_{w,d} \phi_2 & \int_E \mathbf{K} \nabla_{w,d} \phi_0 \cdot \nabla_{w,d} \phi_3 & \int_E \mathbf{K} \nabla_{w,d} \phi_0 \cdot \nabla_{w,d} \phi_4 \\ \int_E \mathbf{K} \nabla_{w,d} \phi_1 \cdot \nabla_{w,d} \phi_0 & \int_E \mathbf{K} \nabla_{w,d} \phi_1 \cdot \nabla_{w,d} \phi_1 & \int_E \mathbf{K} \nabla_{w,d} \phi_1 \cdot \nabla_{w,d} \phi_2 & \int_E \mathbf{K} \nabla_{w,d} \phi_1 \cdot \nabla_{w,d} \phi_3 & \int_E \mathbf{K} \nabla_{w,d} \phi_1 \cdot \nabla_{w,d} \phi_4 \\ \int_E \mathbf{K} \nabla_{w,d} \phi_2 \cdot \nabla_{w,d} \phi_0 & \int_E \mathbf{K} \nabla_{w,d} \phi_2 \cdot \nabla_{w,d} \phi_1 & \int_E \mathbf{K} \nabla_{w,d} \phi_2 \cdot \nabla_{w,d} \phi_2 & \int_E \mathbf{K} \nabla_{w,d} \phi_2 \cdot \nabla_{w,d} \phi_3 & \int_E \mathbf{K} \nabla_{w,d} \phi_2 \cdot \nabla_{w,d} \phi_4 \\ \int_E \mathbf{K} \nabla_{w,d} \phi_3 \cdot \nabla_{w,d} \phi_0 & \int_E \mathbf{K} \nabla_{w,d} \phi_3 \cdot \nabla_{w,d} \phi_1 & \int_E \mathbf{K} \nabla_{w,d} \phi_3 \cdot \nabla_{w,d} \phi_2 & \int_E \mathbf{K} \nabla_{w,d} \phi_3 \cdot \nabla_{w,d} \phi_3 & \int_E \mathbf{K} \nabla_{w,d} \phi_3 \cdot \nabla_{w,d} \phi_4 \\ \int_E \mathbf{K} \nabla_{w,d} \phi_4 \cdot \nabla_{w,d} \phi_0 & \int_E \mathbf{K} \nabla_{w,d} \phi_4 \cdot \nabla_{w,d} \phi_1 & \int_E \mathbf{K} \nabla_{w,d} \phi_4 \cdot \nabla_{w,d} \phi_2 & \int_E \mathbf{K} \nabla_{w,d} \phi_4 \cdot \nabla_{w,d} \phi_3 & \int_E \mathbf{K} \nabla_{w,d} \phi_4 \cdot \nabla_{w,d} \phi_4 \end{bmatrix}. \quad (3.42)$$

We find that $(\nabla_{w,d} \phi_0, \nabla_{w,d} \phi_0)_E$ is the interaction of the element itself, $(\nabla_{w,d} \phi_0, \nabla_{w,d} \phi_i)_E$ ($i = 1, 2, 3, 4$) are interactions of the element and its edges, $(\nabla_{w,d} \phi_i, \nabla_{w,d} \phi_j)_E$ ($i, j = 1, 2, 3, 4$) are interactions of four edges.

From Equation (3.21), we define

$$\nabla_{w,d} \phi_i = c_1 \mathbf{w}_1 + c_2 \mathbf{w}_2 + c_3 \mathbf{w}_3 + c_4 \mathbf{w}_4 = \begin{bmatrix} c_1 + c_3 X \\ c_2 + c_4 Y \end{bmatrix}, \quad (3.43)$$

$$\nabla_{w,d} \phi_j = d_1 \mathbf{w}_1 + d_2 \mathbf{w}_2 + d_3 \mathbf{w}_3 + d_4 \mathbf{w}_4 = \begin{bmatrix} d_1 + d_3 X \\ d_2 + d_4 Y \end{bmatrix}, \quad i, j = 0, 1, 2, 3, 4 \quad (3.44)$$

and $c_1, \dots, c_4, d_1, \dots, d_4$ have been calculated from Equation (3.21).

So for the components of the element stiffness matrix, we have

$$\begin{aligned} \mathbf{K} \nabla_{w,d} \phi_i \cdot \nabla_{w,d} \phi_j &= \begin{bmatrix} K_{11} & K_{12} \\ K_{21} & K_{22} \end{bmatrix} \begin{bmatrix} c_1 + c_3 X \\ c_2 + c_4 Y \end{bmatrix} \cdot \begin{bmatrix} d_1 + d_3 X \\ d_2 + d_4 Y \end{bmatrix} \\ &= \begin{bmatrix} K_{11}(c_1 + c_3 X) + K_{12}(c_2 + c_4 Y) \\ K_{21}(c_1 + c_3 X) + K_{22}(c_2 + c_4 Y) \end{bmatrix} \cdot \begin{bmatrix} d_1 + d_3 X \\ d_2 + d_4 Y \end{bmatrix}, \end{aligned} \quad (3.45)$$

and

$$(\mathbf{K}\nabla_{w,d}\phi_i, \nabla_{w,d}\phi_j)_E = [c_1, \dots, c_4] \begin{bmatrix} \int_E K_{11} & \int_E K_{21} & \int_E K_{11}X & \int_E K_{21}Y \\ \int_E K_{12} & \int_E K_{22} & \int_E K_{12}X & \int_E K_{22}Y \\ \int_E K_{11}X & \int_E K_{21}X & \int_E K_{11}X^2 & \int_E K_{21}XY \\ \int_E K_{12}Y & \int_E K_{22}Y & \int_E K_{12}XY & \int_E K_{22}Y^2 \end{bmatrix} \begin{bmatrix} d_1 \\ \vdots \\ d_4 \end{bmatrix}. \quad (3.46)$$

We derive element-level small matrices which are interactions of the discrete weak gradients. In implementation, we use these small matrices to assemble the sparse global stiffness matrix,

$$\begin{bmatrix} (\mathbf{K}\nabla_{w,d}\Phi_1, \nabla_{w,d}\Phi_1)_\Omega \cdots (\mathbf{K}\nabla_{w,d}\Phi_1, \nabla\Phi_n)_\Omega & (\mathbf{K}\nabla_{w,d}\Phi_1, \nabla\Phi_{n+1})_\Omega \cdots (\mathbf{K}\nabla_{w,d}\Phi_1, \nabla\Phi_m)_\Omega \\ (\mathbf{K}\nabla_{w,d}\Phi_2, \nabla_{w,d}\Phi_1)_\Omega \cdots (\mathbf{K}\nabla_{w,d}\Phi_2, \nabla\Phi_n)_\Omega & (\mathbf{K}\nabla_{w,d}\Phi_2, \nabla\Phi_{n+1})_\Omega \cdots (\mathbf{K}\nabla_{w,d}\Phi_2, \nabla\Phi_m)_\Omega \\ \vdots & \\ (\mathbf{K}\nabla_{w,d}\Phi_m, \nabla_{w,d}\Phi_1)_\Omega \cdots (\mathbf{K}\nabla_{w,d}\Phi_m, \nabla\Phi_n)_\Omega & (\mathbf{K}\nabla_{w,d}\Phi_m, \nabla\Phi_{n+1})_\Omega \cdots (\mathbf{K}\nabla_{w,d}\Phi_m, \nabla\Phi_m)_\Omega \end{bmatrix}, \quad (3.47)$$

where $(\mathbf{K}\nabla_{w,d}\Phi_i, \nabla_{w,d}\Phi_j)_\Omega (i, j = 1, 2, \dots, n)$ are interactions of elements themselves, $(\mathbf{K}\nabla_{w,d}\Phi_i, \nabla_{w,d}\Phi_j)_\Omega (i = 1, \dots, n, j = n+1, \dots, m)$ are interactions of elements and edges, $(\mathbf{K}\nabla_{w,d}\Phi_i, \nabla_{w,d}\Phi_j)_\Omega (i, j = n+1, \dots, m)$ are interactions of all edges. So we extract these interactions from all local matrices (3.42) and assign them into the global stiffness matrix.

We denote the global stiffness matrix as a blocked matrix,

$$\begin{bmatrix} A_{ee} & A_{eg} \\ A_{ge} & A_{gg} \end{bmatrix}, \quad (3.48)$$

where components in the block A_{ee} are interactions among elements. Since each element only interacts with itself, A_{ee} is diagonal. A_{eg} reflects interactions of elements and their edges, A_{ge} is the transpose of A_{eg} , and A_{gg} reflects interactions of all edges. The global stiffness

matrix is a sparse SPD matrix. The WG finite element scheme of the Darcy with homogenous Dirichlet boundary conditions on the entire boundary is

$$\begin{bmatrix} A_{ee} & A_{eg} \\ A_{ge} & A_{gg} \end{bmatrix} \begin{bmatrix} a_1 \\ \vdots \\ a_n \\ a_{n+1} \\ \vdots \\ a_m \end{bmatrix} = \begin{bmatrix} \int_E f dE \\ \vdots \\ \int_E f dE \\ 0 \\ \vdots \\ 0 \end{bmatrix} \quad (3.49)$$

where a_1, \dots, a_n are numerical pressure in interiors and a_{n+1}, \dots, a_m are numerical pressure on edges, the right hand side is calculated in (3.41).

Darcy velocity In the space $RT_{[0]}$, the velocity of quadrilateral elements is a linear combination of basis functions of $RT_{[0]}$, and the velocity $\mathbf{u}_h = c_1 \mathbf{w}_1 + c_2 \mathbf{w}_2 + c_3 \mathbf{w}_3 + c_4 \mathbf{w}_4$.

On each element, numerical pressure $p_h = a_0 \phi_0 + a_1 \phi_1 + a_2 \phi_2 + a_3 \phi_3 + a_4 \phi_4$, ∇p can be approximated by five discrete weak gradients $\nabla_{w,d} \phi_0, \nabla_{w,d} \phi_1, \nabla_{w,d} \phi_2, \nabla_{w,d} \phi_3, \nabla_{w,d} \phi_4$,

$$\nabla_{w,d} p_h = \sum_{i=0}^4 a_i \nabla_{w,d} \phi_i. \quad (3.50)$$

And $\nabla_{w,d} \phi_i = \sum_{j=1}^4 b_{ij} \mathbf{w}_j$, so

$$\nabla_{w,d} p_h = \sum_{i=0}^4 a_i \sum_{j=1}^4 b_{ij} \mathbf{w}_j = \sum_{i=0}^4 \sum_{j=1}^4 a_i b_{ij} \mathbf{w}_j, \quad (3.51)$$

where a_i are results of Equation (3.49), b_{ij} are results of Equation (3.21).

The numerical velocity $\mathbf{u}_h = -\mathbf{K} \nabla_{w,d} p_h$. So

$$\mathbf{u}_h = -\mathbf{K} \nabla_{w,d} p_h = - \sum_{i=0}^4 \sum_{j=1}^4 a_i b_{ij} \mathbf{K} \mathbf{w}_j. \quad (3.52)$$

When \mathbf{K} is a diagonal matrix, $\mathbf{K}\mathbf{w}_j$ is in the space $RT_{[0]}$. The projection can be omitted. When \mathbf{K} is a non-diagonal matrix, then $\mathbf{K}\mathbf{w}_j$ is not in the space $RT_{[0]}$. Thus, we need to project it back to the space.

For example, $\mathbf{K} = \begin{bmatrix} K_{11} & K_{12} \\ K_{21} & K_{22} \end{bmatrix}$, test function in $RT_{[0]}$ is $\mathbf{u} = \begin{bmatrix} a + cx \\ b + dy \end{bmatrix}$. So

$$\mathbf{K}\mathbf{u} = \begin{bmatrix} K_{11} & K_{12} \\ K_{21} & K_{22} \end{bmatrix} \begin{bmatrix} a + cx \\ b + dy \end{bmatrix} = \begin{bmatrix} K_{11}a + K_{12}b + K_{11}cx + K_{12}dy \\ K_{12}a + K_{22}b + K_{12}cx + K_{22}dy \end{bmatrix}. \quad (3.53)$$

The first component of this vector is no longer a linear function of the first variable, and the second component of this vector is no longer a linear function of the second variable, so $\mathbf{K}\mathbf{u}$ is clearly not in $RT_{[0]}$ space. Here, we use L_2 -projection.

Projection Use local L_2 -projection to project $\mathbf{u} \in L^2(\Omega)^2$ into $RT_{[0]}(E)$, that is, let $\mathbf{Q}_h(\mathbf{u}) \in RT_{[0]}(E)$. On a quadrilateral element E ,

$$\mathbf{Q}_h(\mathbf{u}) = c_1\mathbf{w}_1 + c_2\mathbf{w}_2 + c_3\mathbf{w}_3 + c_4\mathbf{w}_4, \quad (3.54)$$

where $\mathbf{w}_i (i = 1, 2, 3, 4)$ are basis functions of $RT_{[0]}(E)$.

Definition

$$\int_E \mathbf{Q}_h(\mathbf{u}) \cdot \mathbf{w}_i = \int_E \mathbf{u} \cdot \mathbf{w}_i.$$

Substituting $\mathbf{Q}_h(\mathbf{u})$ by Equation (3.54), we have the following linear system to solve for the coefficients,

$$\begin{bmatrix} (\mathbf{w}_1, \mathbf{w}_1) & (\mathbf{w}_1, \mathbf{w}_2) & (\mathbf{w}_1, \mathbf{w}_3) & (\mathbf{w}_1, \mathbf{w}_4) \\ (\mathbf{w}_2, \mathbf{w}_1) & (\mathbf{w}_2, \mathbf{w}_2) & (\mathbf{w}_2, \mathbf{w}_3) & (\mathbf{w}_2, \mathbf{w}_4) \\ (\mathbf{w}_3, \mathbf{w}_1) & (\mathbf{w}_3, \mathbf{w}_2) & (\mathbf{w}_3, \mathbf{w}_3) & (\mathbf{w}_3, \mathbf{w}_4) \\ (\mathbf{w}_4, \mathbf{w}_1) & (\mathbf{w}_4, \mathbf{w}_2) & (\mathbf{w}_4, \mathbf{w}_3) & (\mathbf{w}_4, \mathbf{w}_4) \end{bmatrix} \begin{bmatrix} c_1 \\ c_2 \\ c_3 \\ c_4 \end{bmatrix} = \begin{bmatrix} (\mathbf{u}, \mathbf{w}_1) \\ (\mathbf{u}, \mathbf{w}_2) \\ (\mathbf{u}, \mathbf{w}_3) \\ (\mathbf{u}, \mathbf{w}_4) \end{bmatrix}.$$

We define the projection as $\mathbf{Q}_h(\mathbf{K}\mathbf{w}_j) = \sum_{k=1}^4 d_{jk}\mathbf{w}_k$. For any j , $(\mathbf{Q}_h(\mathbf{K}\mathbf{w}_j), \mathbf{w}_k)_E = (\mathbf{K}\mathbf{w}_j, \mathbf{w}_k)_E$. So the numerical velocity becomes

$$\mathbf{u}_h = \mathbf{Q}_h(-\mathbf{K}\nabla_{w,d}p_h) = -\sum_{i=0}^4 \sum_{j=1}^4 a_i b_{ij} \mathbf{Q}_h(\mathbf{K}\mathbf{w}_j). \quad (3.55)$$

and we have the following linear system to solve for the coefficients d_{jk} ,

$$\begin{bmatrix} (\mathbf{w}_1, \mathbf{w}_1) & (\mathbf{w}_1, \mathbf{w}_2) & (\mathbf{w}_1, \mathbf{w}_3) & (\mathbf{w}_1, \mathbf{w}_4) \\ (\mathbf{w}_2, \mathbf{w}_1) & (\mathbf{w}_2, \mathbf{w}_2) & (\mathbf{w}_2, \mathbf{w}_3) & (\mathbf{w}_2, \mathbf{w}_4) \\ (\mathbf{w}_3, \mathbf{w}_1) & (\mathbf{w}_3, \mathbf{w}_2) & (\mathbf{w}_3, \mathbf{w}_3) & (\mathbf{w}_3, \mathbf{w}_4) \\ (\mathbf{w}_4, \mathbf{w}_1) & (\mathbf{w}_4, \mathbf{w}_2) & (\mathbf{w}_4, \mathbf{w}_3) & (\mathbf{w}_4, \mathbf{w}_4) \end{bmatrix} \begin{bmatrix} d_{j1} \\ d_{j2} \\ d_{j3} \\ d_{j4} \end{bmatrix} = \begin{bmatrix} (\mathbf{K}\mathbf{w}_j, \mathbf{w}_1) \\ (\mathbf{K}\mathbf{w}_j, \mathbf{w}_2) \\ (\mathbf{K}\mathbf{w}_j, \mathbf{w}_3) \\ (\mathbf{K}\mathbf{w}_j, \mathbf{w}_4) \end{bmatrix}, \quad (3.56)$$

where the Gram matrix of $RT_{[0]}$ is calculated in the previous section.

So for the elementwise velocity

$$\mathbf{u}_h = -\sum_{i=0}^4 \sum_{j=1}^4 a_i b_{ij} \sum_{k=1}^4 d_{jk} \mathbf{w}_k = \sum_{k=1}^4 -\left(\sum_{j=1}^4 \sum_{i=0}^4 a_i b_{ij} d_{jk}\right) \mathbf{w}_k. \quad (3.57)$$

Bulk normal flux After we've calculated the velocity, we use it to approximate the numerical flux

$$\int_e \mathbf{u}_h \cdot \mathbf{n} = \mathbf{u}_h \cdot \mathbf{n}|e|, \quad (3.58)$$

where \mathbf{u}_h is the numerical velocity at the edge's midpoint, \mathbf{n} is the outward unit vector, $|e|$ is the edge length. The velocity on the quadrilateral is

$$\mathbf{u}_h = c_1 \mathbf{w}_1 + c_2 \mathbf{w}_2 + c_3 \mathbf{w}_3 + c_4 \mathbf{w}_4 = \begin{pmatrix} c_1 + c_3 X \\ c_2 + c_4 Y \end{pmatrix}. \quad (3.59)$$

And

$$\mathbf{n}|e| = \begin{bmatrix} y_{i+1} - y_i \\ -(x_{i+1} - x_i) \end{bmatrix}, \quad (3.60)$$

$$\mathbf{u}_h \cdot \mathbf{n}|_e = \begin{bmatrix} c_1 + c_3(x - x_c) \\ c_2 + c_4(y - y_c) \end{bmatrix} \cdot \begin{bmatrix} y_{i+1} - y_i \\ -(x_{i+1} - x_i) \end{bmatrix}, \quad (3.61)$$

where (x_c, y_c) is the center of the quadrilateral element.

3.5 NUMERICAL RESULTS ON QUADRILATERAL MESHES

In this section, we will show numerical experiments by WG finite element methods on quadrilateral meshes.

Quadrilateral meshes Here, we consider five types of quadrilateral meshes,

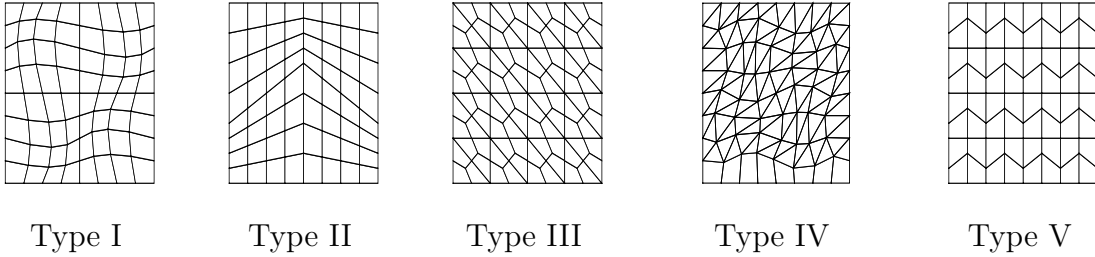


Figure 3.4: Five types of meshes.

- Type I meshes are logically rectangular meshes which are derived from perturbed rectangular meshes.
- Type II meshes are asymptotically parallelogram trapezoidal meshes [4]. In this family of quadrilateral meshes, let θ_1 be the angle between the outward normal vectors of opposite two sides and θ_2 be the angle between the other sides. We define $\sigma_k = \max(|\pi - \theta_1|, |\pi - \theta_2|)$ and h_k to be the diameter of convex quadrilateral element E . For all elements in the mesh, if $\frac{\sigma_k}{h_k}$ is uniformly bounded ($\frac{\sigma_k}{h_k} \leq C$), [4] then this family of quadrilateral meshes is called asymptotically parallelogram quadrilateral. Any polygon can be meshed into an asymptotically parallelogram trapezoidal mesh.
- Type III are quadrilateral meshes obtained from triangular meshes. We create a new

node at the center of each triangle, a new node at the midpoint of each original edge, and connect the new centroid with new midpoints on each triangle.

- Type IV meshes are hybrid meshes consisting of quadrilateral elements and triangular elements.
- Type V meshes are trapezoid meshes.

In this thesis, we mainly discuss Type I, II, III, IV meshes.

Smooth solution The exact pressure is $p = \sin^2(\pi x) \sin(\pi y)$, $f = 2\pi^2 \cos(\pi x) \sin(\pi y)$, in the domain $\Omega = (0, 1)^2$. We test it on the logically rectangular meshes, which are adopted from [30]. Specifically, the quadrilateral mesh points are

$$\begin{cases} x = \hat{x} + 0.06 \sin(2\pi\hat{x}) \sin(2\pi\hat{y}), \\ y = \hat{y} - 0.05 \sin(2\pi\hat{x}) \sin(2\pi\hat{y}), \end{cases}$$

where (\hat{x}, \hat{y}) are the corresponding rectangular mesh points. We also test it on a quadrilateral mesh which is refined from a triangular mesh.

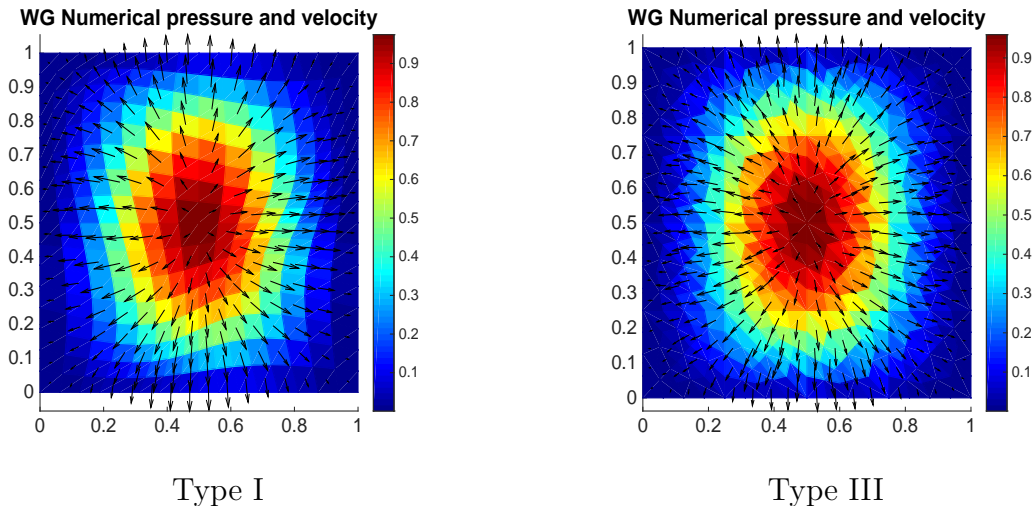


Figure 3.5: Smooth solution: Numerical pressure and velocity from the WGFEMs on a logically rectangular mesh (left) and a quadrilateral mesh (right). Both have mesh size $h = 1/16$.

Table 3.1: Smooth solution example: Numerical results of $WG(Q_0, Q_0; RT_{[0]})$ method on quadrilateral meshes

$1/h$	$\ p - p_h^\circ\ $	$\ \mathbf{u} - \mathbf{u}_h\ $	$\ (\mathbf{u} - \mathbf{u}_h) \cdot \mathbf{n}\ $	$\min(p_h^\circ)$	$\max(p_h^\circ)$
Type I meshes					
8	7.9787e-02	2.9333e-01	3.9052e-01	4.9321e-03	9.1103e-01
16	3.9992e-02	1.4134e-01	1.9217e-01	7.9909e-04	9.7451e-01
32	2.0008e-02	6.9866e-02	9.5649e-02	1.2073e-04	9.9313e-01
64	1.0006e-02	3.4827e-02	4.7769e-02	1.6882e-05	9.9822e-01
Conv.rate	0.998	1.024	1.01	N/A	N/A
Type IV meshes					
8	7.8950e-02	7.1381e-01	9.2420e-01	-5.4381e-03	8.6684e-01
16	3.6052e-02	3.5510e-01	4.6914e-01	9.1560e-04	9.5896e-01
32	1.7429e-02	1.6021e-01	2.1262e-01	1.4879e-04	9.9110e-01
64	8.6739e-03	7.3582e-02	9.8494e-02	2.0641e-05	9.9823e-01
Conv.rate	1.062	1.092	1.076	N/A	N/A

The exact solution for pressure is $p = \sin^2(\pi x) \sin(\pi y)$, it is easy to see that the maximum is 1 and the minimum is 0. From the table, with the better refinement of the quadrilateral mesh, the $\min(\text{NumerPresEm})$ is getting closer to 0 and the $\max(\text{NumerPresEm})$ is getting closer to 1. There is no singularities in the domain, so the convergence rates of pressure, velocity and flux are around 1.

Lower regularity solution In the domain $\Omega = (0, 1)^2$, $\mathbf{K} = \mathbf{I}_2$, the analytic equation for pressure is

$$p(x, y) = x(1-x)y(1-y)(\sqrt{x^2 + y^2})^{-(2-a)},$$

and the source term

$$f = - (x^2 + y^2)^{(-2+0.5a)}(2x^4 - 2x^3 + (-a^2 + 6 - 2a)x^2y + (a^2 - 8 + 4a)x^2y^2 + (a^2 - 4)xy + (-a^2 + 6 - 2a)xy^2 + 2y^4 - 2y^3),$$

with homogeneous Dirichlet boundary conditions on the entire boundary. The pressure allows a corner singularity at the origin, so the function is with a lower regularity. For the test example, we take the regularity parameter $a = \frac{1}{3}$.

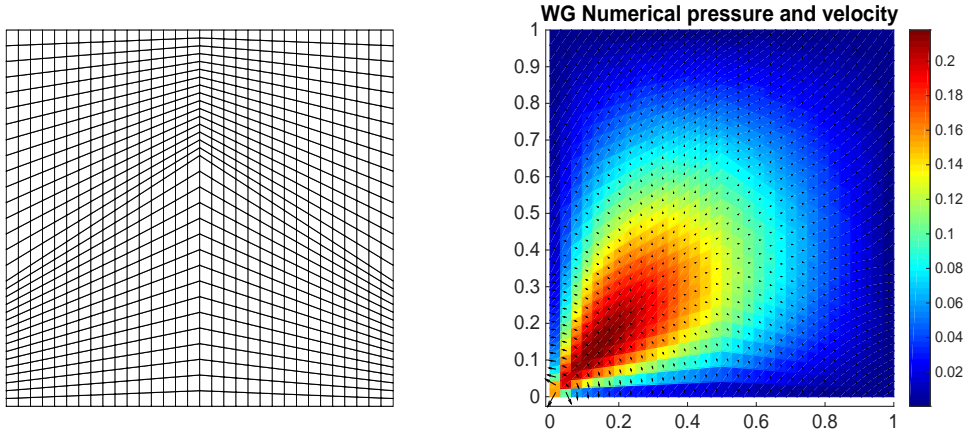


Figure 3.6: Lower regularity solution: Numerical pressure and velocity from the lowest-order weak Galerkin method on a asymptotically parallelogram mesh with mesh size $h = 1/32$.

Table 3.2: Low regularity example: Numerical results of $WG(Q_0, Q_0; RT_{[0]})$ method on asymptotically parallelogram quadrilateral meshes

$1/h$	$\ p - p_h^\circ\ $	$\ \mathbf{u} - \mathbf{u}_h\ $	$\ (\mathbf{u} - \mathbf{u}_h) \cdot \mathbf{n}\ $	$\min(p_h^\circ)$	$\max(p_h^\circ)$
8	2.67E-02	5.0765E-01	1.6957E+00	2.5994E-03	2.6493E-01
16	1.2341E-02	3.9273E-01	1.3020E+00	6.7727E-04	2.3842E-01
32	5.9880E-03	3.0796E-01	1.0164E+00	1.7388E-04	2.1801E-01
64	2.9648E-03	2.4305E-01	8.0019E-01	4.2116E-05	2.1582E-01
128	1.4782E-03	1.9239E-01	6.3256E-01	1.0354E-05	2.1564E-01
Conv.rate	1.043	0.349	0.355	N/A	N/A

Table (3.2) shows that the pressure error is with first order convergence. As for the convergence rates of velocity and flux error, we take the ratio of the former error and the later error, denote it as c , then calculate $\log_2(c)$ which is the convergence rate. And the convergence rates of velocity and flux are around $\frac{1}{3}$. This result verifies the proposition (3.30), which stated that if the domain or the function is with a lower regularity, the convergence rates of velocity and flux are around that regularity parameter.

3.6 LOWEST ORDER WGFEMs ON HYBRID MESHES

In previous sections, we showed how to use WGFEMs to solve the Darcy equation on quadrilateral meshes. Here, we will see that WGFEMs can also be used for solving the Darcy equation on hybrid meshes, which consist of quadrilaterals and triangles [1].

We test a simple example. The exact solution for the pressure is $p = \sin(\pi x) \sin(\pi y)$. On

the domain $\Omega = (0, 1)^2$, $\mathbf{K} = \mathbf{I}_2$ and a homogeneous Dirichlet boundary condition on the entire boundary. The following figure is the numerical pressure and velocity in the hybrid mesh with mesh size $h = \frac{1}{16}$.

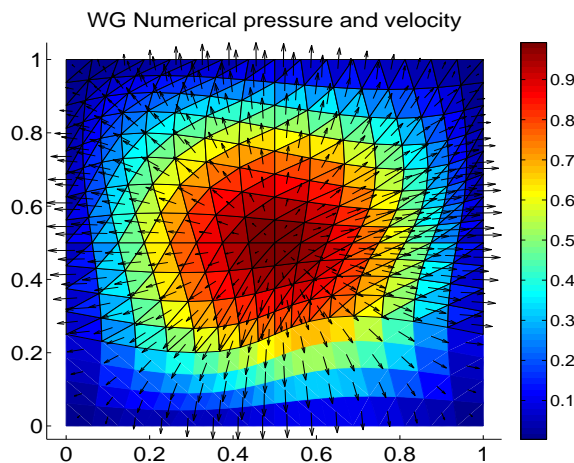


Figure 3.7: Numerical pressure and velocity from WGFEMs on a hybrid mesh with mesh size $h = 1/16$, see [24]

Table 3.3: Example: Numerical results of $\text{WG}(Q_0, Q_0; RT_{[0]})$ method on hybrid meshes, results from [24]

$1/h$	$\ p - p_h^\circ\ $	$\ \mathbf{u} - \mathbf{u}_h\ $	$\ (\mathbf{u} - \mathbf{u}_h) \cdot \mathbf{n}\ $	$\min(p_h^\circ)$	$\max(p_h^\circ)$
8	7.2665e-2	2.7675e-1	3.3213e-1	1.3150e-2	9.6983e-1
16	3.6563e-2	1.3839e-1	1.6405e-1	3.3015e-3	9.9233e-1
32	1.8311e-2	6.9195e-2	8.1719e-2	8.1269e-4	9.9807e-1
64	9.1592e-3	3.4598e-2	4.0817e-2	2.0159e-4	9.9952e-1
Conv.rate	0.995	0.999	1.008	N/A	N/A

The table (3.3) shows the errors of lowest order WGFEMs on hybrid meshes. Convergence rates in pressure, velocity and flux are seen to be first order.

CHAPTER 4

WGFEMS ON HEXAHEDRAL MESHES

In previous chapters, we showed how to use WGFEMs to solve the Darcy equation on quadrilateral and hybrid meshes. In this chapter, we discuss the lowest order WGFEMs for the Darcy equation on hexahedral meshes and present some numerical results. Readers are referred to [18] for further details of the construction of meshes.

4.1 WG $(Q_0, Q_0; RT_{[0]})$ ELEMENTS ON HEXAHEDRA

On a hexahedron E , the local Raviart-Thomas space is defined as

$$RT_{[0]}(E) = \text{Span}(\mathbf{w}_1, \mathbf{w}_2, \mathbf{w}_3, \mathbf{w}_4, \mathbf{w}_5, \mathbf{w}_6), \quad (4.1)$$

where (x_c, y_c, z_c) is the center of the hexahedron, and $X = x - x_c, Y = y - y_c, Z = z - z_c$,

$$\mathbf{w}_1 = \begin{bmatrix} 1 \\ 0 \\ 0 \end{bmatrix}, \mathbf{w}_2 = \begin{bmatrix} 0 \\ 1 \\ 0 \end{bmatrix}, \mathbf{w}_3 = \begin{bmatrix} 0 \\ 0 \\ 1 \end{bmatrix}, \mathbf{w}_4 = \begin{bmatrix} X \\ 0 \\ 0 \end{bmatrix}, \mathbf{w}_5 = \begin{bmatrix} 0 \\ Y \\ 0 \end{bmatrix}, \mathbf{w}_6 = \begin{bmatrix} 0 \\ 0 \\ Z \end{bmatrix}.$$

The Gram matrix of the above basis is a 6×6 symmetric positive-definite (SPD) matrix.

Definitions of weak functions, weak gradients, discrete weak functions and discrete weak gradients are similar to those defined in Chapter 3. On the hexahedron E , seven discrete weak functions are defined in the interior and on the six faces of the element respectively,

- $\phi_0 = 1$ in the interior E° , $\phi_0 = 0$ on the boundary E^∂ ;
- $\phi_i = 1 (i = 1, 2, \dots, 6)$ on the very face, $\phi_i = 0$ on all other five faces and in the interior.

The discrete weak gradient $\nabla_{w,d}\phi$ is again specified in $RT_{[0]}(E)$ via integration by parts,

$$\int_E (\nabla_{w,d}\phi) \cdot \mathbf{w} = \int_{E^\partial} \phi^\partial(\mathbf{w} \cdot \mathbf{n}) - \int_{E^\circ} \phi^\circ(\nabla \cdot \mathbf{w}), \quad \forall \mathbf{w} \in RT_{[0]}(E). \quad (4.2)$$

The discrete weak gradients of the seven basis functions for the pressure are specified in the local $RT_{[0]}$ space as

$$\nabla_{w,d}\phi_i = c_{i1}\mathbf{w}_1 + c_{i2}\mathbf{w}_2 + c_{i3}\mathbf{w}_3 + c_{i4}\mathbf{w}_4 + c_{i5}\mathbf{w}_5 + c_{i6}\mathbf{w}_6, \quad i = 0, 1, 2, 3, \dots, 6.$$

As in Section 3.1.1, 3.1.2, we use Equation (4.2) and definitions of ϕ_i to solve for the coefficients.

Specifically, when E is a brick, we have

$$\left\{ \begin{array}{l} \nabla_{w,d}\phi_0 = \quad 0\mathbf{w}_1 \quad + \quad 0\mathbf{w}_2 \quad + \quad 0\mathbf{w}_3 \quad + \quad \frac{-12}{(x_1-x_0)^2}\mathbf{w}_4 \quad + \quad \frac{-12}{(y_1-y_0)^2}\mathbf{w}_5 \quad + \quad \frac{-12}{(z_1-z_0)^2}\mathbf{w}_6, \\ \nabla_{w,d}\phi_1 = \quad \frac{-1}{x_1-x_0}\mathbf{w}_1 \quad + \quad 0\mathbf{w}_2 \quad + \quad 0\mathbf{w}_3 \quad + \quad \frac{6}{(x_1-x_0)^2}\mathbf{w}_4 \quad + \quad 0\mathbf{w}_5 \quad + \quad 0\mathbf{w}_6, \\ \nabla_{w,d}\phi_2 = \quad \frac{1}{x_1-x_0}\mathbf{w}_1 \quad + \quad 0\mathbf{w}_2 \quad + \quad 0\mathbf{w}_3 \quad + \quad \frac{6}{(x_1-x_0)^2}\mathbf{w}_4 \quad + \quad 0\mathbf{w}_5 \quad + \quad 0\mathbf{w}_6, \\ \nabla_{w,d}\phi_3 = \quad 0\mathbf{w}_1 \quad + \quad \frac{-1}{y_1-y_0}\mathbf{w}_2 \quad + \quad 0\mathbf{w}_3 \quad + \quad 0\mathbf{w}_4 \quad + \quad \frac{6}{(y_1-y_0)^2}\mathbf{w}_5 \quad + \quad 0\mathbf{w}_6, \\ \nabla_{w,d}\phi_4 = \quad 0\mathbf{w}_1 \quad + \quad \frac{1}{y_1-y_0}\mathbf{w}_2 \quad + \quad 0\mathbf{w}_3 \quad + \quad 0\mathbf{w}_4 \quad + \quad \frac{6}{(y_1-y_0)^2}\mathbf{w}_5 \quad + \quad 0\mathbf{w}_6, \\ \nabla_{w,d}\phi_5 = \quad 0\mathbf{w}_1 \quad + \quad 0\mathbf{w}_2 \quad + \quad \frac{-1}{z_1-z_0}\mathbf{w}_3 \quad + \quad 0\mathbf{w}_4 \quad + \quad 0\mathbf{w}_5 \quad + \quad \frac{6}{(z_1-z_0)^2}\mathbf{w}_6, \\ \nabla_{w,d}\phi_6 = \quad 0\mathbf{w}_1 \quad + \quad 0\mathbf{w}_2 \quad + \quad \frac{1}{z_1-z_0}\mathbf{w}_3 \quad + \quad 0\mathbf{w}_4 \quad + \quad 0\mathbf{w}_5 \quad + \quad \frac{6}{(z_1-z_0)^2}\mathbf{w}_6. \end{array} \right.$$

4.2 LOWEST ORDER WG SCHEME FOR DARCY ON HEXAHEDRA

In this section, we show how to use $WG(Q_0, Q_0; RT_{[0]})$, the lowest order WG finite elements, to construct a finite element scheme on a hexahedral mesh and solve the Darcy equation (1.2).

Let \mathcal{E}_h be a hexahedral mesh for a three-dimensional polyhedral domain Ω , S_h and S_h^0 be spaces of discrete weak functions over this mesh, defined in a similar way to Equation (3.4), (3.5).

WG($Q_0, Q_0; RT_{[0]}$) for the Darcy equation on a hexahedral mesh: Seek $p_h = \{p_h^\circ, p_h^\partial\} \in S_h$, where p_h° is a set of numerical pressure values in all elements' interiors, p_h^∂ is a set of numerical pressure values on all faces, such that $p_h^\partial|_{\Gamma_h^D} = \mathbf{Q}_h^\partial(p_D)$ (the L^2 -projection of the Dirichlet boundary data into the space of all piecewise constant functions on Γ_h^D and

$$\mathcal{A}_h(p_h, q) = \mathcal{F}(q), \quad \forall q = \{q^\circ, q^\partial\} \in S_h^0, \quad (4.3)$$

where

$$\mathcal{A}_h(p_h, q) := \sum_{E \in \mathcal{E}_h} \int_E \mathbf{K} \nabla_{w,d} p_h \cdot \nabla_{w,d} q, \quad (4.4)$$

and

$$\mathcal{F}(q) := \sum_{E \in \mathcal{E}_h} \int_E f q^\circ - \sum_{\gamma \in \Gamma_h^N} \int_\gamma u_N q^\partial. \quad (4.5)$$

This large size sparse SPD linear system will be solved to obtain the numerical pressure.

For the numerical velocity, it is obtained by postprocessing. In particular, on each element, $\mathbf{u}_h = \mathbf{Q}_h(-\mathbf{K} \nabla_{w,d} p_h)$, where \mathbf{Q}_h is an L^2 -projection of $(-\mathbf{K} \nabla_{w,d} p_h)$ into the subspace $RT_{[0]}(E)$. When \mathbf{K} is an elementwise constant scalar matrix, $\mathbf{K} \nabla_{w,d} p_h$ is still in the space $RT_{[0]}(E)$, this projection can be omitted.

This WG finite element scheme still satisfies the two important physical properties and the convergence proposition. The proofs are similar to those in Section 3.4. See [18] for details.

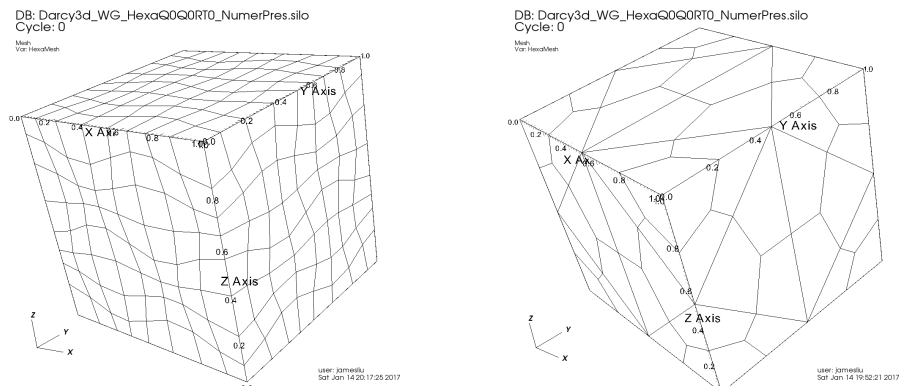
Now we use the following norms

$$\|p - p_h^\circ\|^2 := \sum_{E \in \mathcal{E}_h} \|p - p_h^\circ\|_{L^2(E)}^2, \quad \|\mathbf{u} - \mathbf{u}_h\|^2 := \sum_{E \in \mathcal{E}_h} \|\mathbf{u} - \mathbf{u}_h\|_{L^2(E)^3}^2, \quad (4.6)$$

$$\|(\mathbf{u} - \mathbf{u}_h) \cdot \mathbf{n}\|^2 := \sum_{E \in \mathcal{E}_h} \sum_{\gamma \subset E^\partial} \frac{|E|}{|\gamma|} \|\mathbf{u} \cdot \mathbf{n} - \mathbf{u}_h \cdot \mathbf{n}\|_{L^2(\gamma)}^2, \quad (4.7)$$

where h is the mesh size, $|E|$ is the volume of the hexahedron in the mesh, $|\gamma|$ is the area of any face of the hexahedral element E .

This WG finite element scheme has been tested on hexahedral meshes [18]. Two types of meshes could be used for testing. A type I mesh is obtained from h^2 -perturbations of uniform brick meshes [18], [31]. A type II mesh is the refinement of a tetrahedral mesh by connecting the centroid of each original tetrahedron, the centroid of each original triangular face and the midpoint of each original edge. These meshes are asymptotically parallelepiped [31].



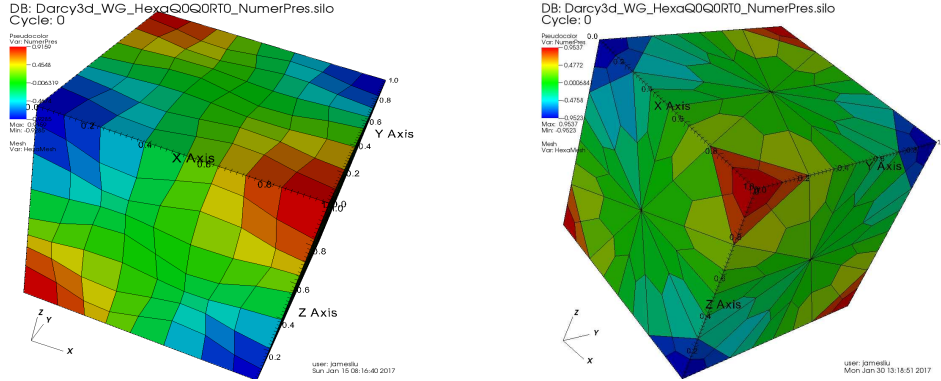
Type I hexahedral meshes, Ref. [18] Type II hexahedral meshes, Ref. [18]

Figure 4.1: Two types of hexahedral meshes [18]. Type I: A logically brick mesh [30]; Type II: Refinement of a tetrahedral mesh into the hexahedral mesh.

Example 1. The exact pressure solution is $p(x, y, z) = \cos(\pi x) \cos(\pi y) \cos(\pi z)$, the source term is $f = 3\pi^2 \cos(\pi x) \cos(\pi y) \cos(\pi z)$, on the domain $\Omega = (0, 1)^3$ (the unit cube) with the exact solution values on Dirichlet boundaries $\Gamma^D = \partial\Omega$, $\mathbf{K} = \mathbf{I}_3$. Figure (4.2) shows the numerical pressures for Type I and II hexahedral meshes. Tables (4.1) and (4.2) are the numerical results from the WG $(Q_0, Q_0; RT_{[0]})$ finite element methods. From the tables, we observe that convergence rates in pressure, velocity, and flux close to the first order.

Table 4.1: Example 1: Convergence rates of errors in pressure, velocity, and flux on the Type I mesh [18]

$1/h$	$\ p - p_h^\circ\ $	$\ \mathbf{u} - \mathbf{u}_h\ $	$\ (\mathbf{u} - \mathbf{u}_h) \cdot \mathbf{n}\ $
8	7.0011E-2	3.2844E-1	7.1386E-2
16	3.5623E-2	1.6527E-1	3.5469E-2
32	1.7905E-2	8.2288E-2	1.7623E-2
64	8.9652E-3	4.1069E-2	8.7969E-3
Conv.rate	0.988	0.999	1.006



Hexahedral meshes Type I, $h = 1/8$ Hexahedral meshes Type II, $h = 1/8$

Figure 4.2: Example 1: Numerical pressure profiles on Type I and II hexahedral meshes [18]

Table 4.2: Example 1: Convergence rates of errors in pressure, velocity, and flux on the Type II mesh [18]

$1/h$	$\ p - p_h^o\ $	$\ \mathbf{u} - \mathbf{u}_h\ $	$\ (\mathbf{u} - \mathbf{u}_h) \cdot \mathbf{n}\ $
4	3.0310E-5	1.2359E-3	2.2008E-4
8	1.4466E-5	5.7003E-4	1.2107E-4
16	7.1904E-6	2.8141E-4	6.2760E-5
32	3.6280E-6	1.4303E-4	3.2173E-5
64	1.8858E-6	7.7412E-5	1.7172E-5
Conv.rate	1.001	0.998	0.920

CHAPTER 5

WGFEMS FOR ELASTICITY

From previous chapters, we see that weak Galerkin finite element methods can be used for solving the Darcy equation on two-dimensional and three-dimensional domains, and they satisfy two important physical properties. We can establish concepts of discrete weak divergence and discrete weak curl also. So WGFEMs can be developed for solving the Stokes equation and the elasticity equation.

In this chapter, we establish weak Galerkin finite element methods for solving the linear elasticity equation,

$$\begin{cases} -\nabla \cdot \sigma(\mathbf{u}) = \mathbf{f}, & \text{in } \Omega, \\ \mathbf{u} = \hat{\mathbf{u}}, & \text{on } \Gamma, \end{cases} \quad (5.1)$$

where \mathbf{u} is the displacement vector, \mathbf{f} is the exterior force, $\hat{\mathbf{u}}$ is boundary value, $\varepsilon(\mathbf{u})$ is the strain tensor,

$$\varepsilon(\mathbf{u}) = \frac{1}{2}(\nabla \mathbf{u} + \nabla(\mathbf{u})^T),$$

$\sigma(\mathbf{u})$ is the stress tensor,

$$\sigma(\mathbf{u}) = 2\mu\varepsilon(\mathbf{u}) + \lambda(\nabla \cdot \mathbf{u})\mathbf{I},$$

λ and μ are Lamé constants, which are material based quantities.

When there is only Dirichlet boundary conditions, we have

$$-(\mu\Delta \mathbf{u} + (\mu + \lambda)\nabla(\nabla \cdot \mathbf{u})) = \mathbf{f}, \quad \text{in } \Omega, \quad (5.2)$$

which is subject to certain boundary conditions.

Before talking about the WG finite element methods, we recall how to calculate the gradient of vectors and divergence of matrices.

For example, $\mathbf{u} = (u_1, u_2)$, then

$$\nabla \mathbf{u} = \begin{bmatrix} \partial_x u_1 & \partial_y u_1 \\ \partial_x u_2 & \partial_y u_2 \end{bmatrix};$$

matrix $A = \begin{bmatrix} a_{11} & a_{12} \\ a_{21} & a_{22} \end{bmatrix}$, then the divergence of the matrix A is

$$\nabla \cdot A = \begin{bmatrix} \partial_x a_{11} + \partial_y a_{12} \\ \partial_x a_{21} + \partial_y a_{22} \end{bmatrix}.$$

Weak divergence. [29] The weak divergence of $\mathbf{v} \in W(E)$, denoted as $\nabla_w \cdot \mathbf{v}$, is a linear functional in the Soblev space $H^1(E)$, so its action on any test function $\phi \in H^1(E)$ is

$$\int_E (\nabla_w \cdot \mathbf{v}) \phi = - \int_{E^\circ} \mathbf{v}^\circ \cdot (\nabla \phi) + \int_{E^\partial} \mathbf{v}^\partial \cdot (\phi \mathbf{n}), \quad (5.3)$$

where $W(E)$ is the space of weak functions in an element E and defined as

$$W(E) = \{\mathbf{v} = \{\mathbf{v}^\circ, \mathbf{v}^\partial\} : \mathbf{v}^\circ \in L^2(E)^2, \mathbf{v}^\partial \in L^2(E^\partial)^2\}, \quad (5.4)$$

and

$$H^1(E) = \{v : v \in L^2(E), \nabla v \in L^2(E)\}, \quad (5.5)$$

\mathbf{v}° is the value of \mathbf{v} defined in E° , \mathbf{v}^∂ is the value of \mathbf{v} defined on the boundary E^∂ , \mathbf{n} is the unit outward normal vector on E^∂ .

Discrete weak divergence. [29] The discrete weak divergence is denoted as $\nabla_{w,d} \cdot \mathbf{v} \in P^r(E)$, satisfying

$$\int_E (\nabla_{w,d} \cdot \mathbf{v}) \phi = - \int_{E^\circ} \mathbf{v}^\circ \cdot (\nabla \phi) + \int_{E^\partial} \mathbf{v}^\partial \cdot (\phi \mathbf{n}), \quad \forall \phi \in P^r(E), \quad (5.6)$$

where ϕ is a scalar-valued degree r polynomial, $\nabla \phi$ is taken in the classical sense, $P^r(E)$ is a set of polynomials on E with degree no larger than r .

Weak gradient. The weak gradient of $\mathbf{v} \in W(E)$, denoted as $\nabla_w \mathbf{v}$, is a linear functional in the Soblev space $H^1(E)^{2 \times 2}$, so its action on $W \in H^1(E)^{2 \times 2}$ is [29]

$$\int_E (\nabla_w \mathbf{v}) : W = - \int_{E^\circ} \mathbf{v}^\circ \cdot (\nabla \cdot W) + \int_{E^\partial} \mathbf{v}^\partial \cdot (W \mathbf{n}), \quad \forall W \in H^1(E)^{2 \times 2}, \quad (5.7)$$

where W is a 2×2 matrix with entries in $H^1(E)$, \mathbf{n} is the outward normal vector on E^∂ .

Discrete weak gradient. The discrete weak gradient $\nabla_{w,d} \mathbf{v}$ is a matrix valued polynomial, such that,

$$\int_E (\nabla_{w,d} \mathbf{v}) : W = - \int_{E^\circ} \mathbf{v}^\circ \cdot (\nabla \cdot W) + \int_{E^\partial} \mathbf{v}^\partial \cdot (W \mathbf{n}), \quad \forall W \in P^r(E)^{2 \times 2}, \quad (5.8)$$

where W is a matrix-valued degree r polynomial.

Weak form. Seek $\mathbf{u} \in H^1(\Omega)^2$,

$$\int_\Omega 2\mu(\varepsilon_w(\mathbf{u}) : \varepsilon_w(\mathbf{v})) + \int_\Omega \lambda(\nabla_w \cdot \mathbf{u})(\nabla_w \cdot \mathbf{v}) = \int_\Omega \mathbf{f} \mathbf{v}, \quad \forall \mathbf{v} \in H_0^1(\Omega)^2, \quad (5.9)$$

$\varepsilon_w(\mathbf{u})$ is the weak strain tensor, $\nabla_w \cdot \mathbf{u}$ is the weak divergence. Use the weak gradient and the weak divergence, the weak strain tensor is defined as

$$\varepsilon_w(\mathbf{v}) = \frac{1}{2} (\nabla_w \mathbf{v} + (\nabla_w \mathbf{v})^T), \quad (5.10)$$

and the weak stress tensor is defined as

$$\sigma_w(\mathbf{v}) = 2\mu\varepsilon_w(\mathbf{v}) + \lambda(\nabla_w \cdot \mathbf{v})\mathbf{I}. \quad (5.11)$$

As for Equation (5.2), the weak form of it is

$$\mu(\nabla_w \mathbf{u}, \nabla_w \mathbf{v}) + (\mu + \lambda)(\nabla_w \cdot \mathbf{u}, \nabla_w \cdot \mathbf{v}) = (\mathbf{f}, \mathbf{v}). \quad (5.12)$$

Let E be a quadrilateral element. We consider the lowest order WG $(Q_0^2, Q_0^2; RT_{[0]}^2, Q_0)$. The first Q_0^2 means that two-dimensional vector-valued polynomials are used to approximate the displacement in the interior; the second Q_0^2 means that two-dimensional vector-valued polynomials are used to approximate the displacement on the boundaries;

$$RT_{[0]}^2 = \text{Span} \left\{ \begin{bmatrix} 1 & 0 \\ 0 & 0 \end{bmatrix}, \begin{bmatrix} 0 & 1 \\ 0 & 0 \end{bmatrix}, \begin{bmatrix} 0 & 0 \\ 1 & 0 \end{bmatrix}, \begin{bmatrix} 0 & 0 \\ 0 & 1 \end{bmatrix}, \begin{bmatrix} X & 0 \\ 0 & 0 \end{bmatrix}, \begin{bmatrix} 0 & Y \\ 0 & 0 \end{bmatrix}, \begin{bmatrix} 0 & 0 \\ X & 0 \end{bmatrix}, \begin{bmatrix} 0 & 0 \\ 0 & Y \end{bmatrix} \right\}; \quad (5.13)$$

the last Q_0 means that the divergence of these vector-valued polynomials are constants.

In Equation (5.6), ϕ is taken as constant 1, so $\nabla\phi = (0, 0)$, then the equation becomes

$$\int_E (\nabla_w \cdot \mathbf{v})\phi = \int_{E^\partial} \mathbf{v}^\partial \cdot (\phi \mathbf{n}). \quad (5.14)$$

In Equation (5.8), W is taken from the following matrices:

$$\begin{bmatrix} 1 & 0 \\ 0 & 0 \end{bmatrix}, \begin{bmatrix} 0 & 1 \\ 0 & 0 \end{bmatrix}, \begin{bmatrix} 0 & 0 \\ 1 & 0 \end{bmatrix}, \begin{bmatrix} 0 & 0 \\ 0 & 1 \end{bmatrix}, \quad (5.15)$$

so $\nabla \cdot W$ is the zero vector. Then the equation becomes

$$\int_E (\nabla_{w,d} \mathbf{v}) : W = \int_{E^\partial} \mathbf{v}^\partial \cdot (W \mathbf{n}). \quad (5.16)$$

The discrete weak function space on each element E is

$$W(E, l, m) = \{\mathbf{v} = (\mathbf{v}^\circ, \mathbf{v}^\partial), \mathbf{v}^\circ \in P^l(E^\circ)^2, \mathbf{v}^\partial \in P^m(E^\partial)^2\}. \quad (5.17)$$

Two spaces of discrete weak functions over the mesh \mathcal{E}_h are

$$S_h = \{\mathbf{v} = \{\mathbf{v}^\circ, \mathbf{v}^\partial\} : \mathbf{v}|_E \in W(E, l, m), \forall E \in \mathcal{E}_h\}, \quad (5.18)$$

$$S_h^0 = \{\mathbf{v} = \{\mathbf{v}^\circ, \mathbf{v}^\partial\} \in S_h, \mathbf{v}^\partial = 0 \text{ on } \Gamma\}. \quad (5.19)$$

WG FE scheme. For a numerical solution of the elasticity equation, find $\mathbf{u}_h = \{\mathbf{u}_h^\circ, \mathbf{u}_h^\partial\} \in S_h$, where \mathbf{u}_h° is the value in E° , \mathbf{u}_h^∂ is the value on E^∂ , and $\mathbf{u}_h^\partial|_{\Gamma_h} = \mathbf{Q}_h^\partial(\mathbf{u}_D)$, such that

$$\mathcal{A}(\mathbf{u}_h, \mathbf{v}) = \mathcal{F}(\mathbf{v}), \quad \forall \mathbf{v} \in S_h^0, \quad (5.20)$$

where

$$\mathcal{A}(\mathbf{u}_h, \mathbf{v}) = \sum_{E \in \mathcal{E}_h} 2\mu(\varepsilon_{w,d}(\mathbf{u}_h), \varepsilon_{w,d}(\mathbf{v}))_E + \sum_{E \in \mathcal{E}_h} \lambda(\nabla_{w,d} \cdot \mathbf{u}_h, \nabla_{w,d} \cdot \mathbf{v})_E, \quad (5.21)$$

$$\mathcal{F}(\mathbf{v}) = \sum_{E \in \mathcal{E}_h} (\mathbf{f}, \mathbf{v})_E. \quad (5.22)$$

CHAPTER 6

CONCLUSION

6.1 OTHER COMBINATIONS FOR WG ELEMENTS

In previous chapters, we have investigated the lowest order weak Galerkin finite element methods for the Darcy equation. Due to the flexibility in constructing weak Galerkin finite elements, we explore other possible combinations for weak Galerkin finite elements.

6.1.1 $WG(Q_1, P_1; RT_{[0]})$ Elements on Quadrilaterals

In this combination, WG basis functions are Q_1 polynomials in element interiors and P_1 polynomials on edges, their discrete weak gradients are in $RT_{[0]}$.

On each quadrilateral element, there are twelve WG basis functions, four for interior: $\phi_{01}, \phi_{02}, \phi_{03}, \phi_{04}$; two for each edge: $\phi_{i1}, \phi_{i2} (i = 1, 2, 3, 4)$, as shown in Figure 6.1:

- $\phi_{0j} = 1, X, Y, XY (j = 1, 2, 3, 4)$ for the interior;
- $\phi_{kl} = 1, r (k = 1, 2, 3, 4; l = 1, 2)$ on each edge.

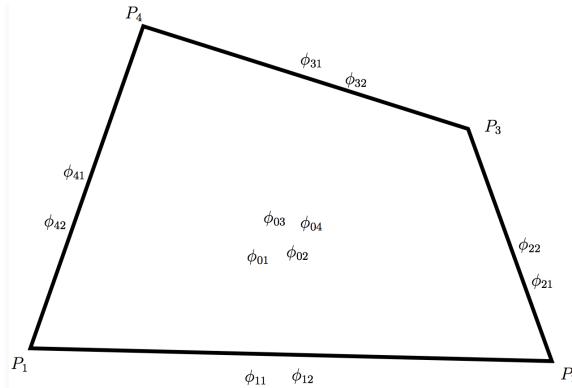


Figure 6.1: Twelve weak Galerkin basis functions on a quadrilateral

We calculate the discrete weak gradients of these basis functions, and then use these discrete weak gradients to approximate the classical gradient. We use this WG method to solve the pressure in the Darcy equation.

In the process of solving the Darcy equation, we use the discrete weak gradients to calculate element stiffness matrices, which are assembled into a global stiffness matrix. For this method, we observed that the global stiffness matrix is singular. We examine further the structures of element stiffness matrices and the global stiffness matrix.

For simplicity, we consider a 2×2 uniform rectangular mesh over the unit square $[0, 1]^2$. On each rectangular element E , we have $\int_E X = 0, \int_E Y = 0, \int_E XY = 0$, where X, Y are the normalized coordinates.

For a rectangular element, the Gram matrix of $RT_{[0]}$ is a diagonal matrix

$$GM = \begin{bmatrix} |E| & 0 & 0 & 0 \\ 0 & |E| & 0 & 0 \\ 0 & 0 & \int_E X^2 & 0 \\ 0 & 0 & 0 & \int_E Y^2 \end{bmatrix}. \quad (6.1)$$

Comparing $WG(Q_1, P_1; RT_{[0]})$ with $WG(Q_0, Q_0; RT_{[0]})$, the difference is that we have three more WG basis functions X, Y, XY defined in the interior and one more basis function r on each edge in $WG(Q_1, P_1; RT_{[0]})$.

For these three new WG basis functions for the element interior (X, Y, XY), we check the right hand sides of the following definition equation:

$$\int_E (\nabla_{w,d}\phi) \cdot \mathbf{w} = \int_{E^\partial} \phi^\partial(\mathbf{w} \cdot \mathbf{n}) - \int_{E^\circ} \phi^\circ(\nabla \cdot \mathbf{w}), \quad \forall \mathbf{w} \in RT_{[0]}(E). \quad (6.2)$$

Clearly, the right hand sides are respectively

$$\begin{bmatrix} 0 \\ 0 \\ -\int_E X \\ -\int_E X \end{bmatrix}, \begin{bmatrix} 0 \\ 0 \\ -\int_E Y \\ -\int_E Y \end{bmatrix}, \begin{bmatrix} 0 \\ 0 \\ -\int_E XY \\ -\int_E XY \end{bmatrix}. \quad (6.3)$$

When E is a rectangular element, $\int_E X = 0, \int_E Y = 0, \int_E XY = 0$. Then the right hand sides become

$$\begin{bmatrix} 0 \\ 0 \\ 0 \\ 0 \end{bmatrix}, \begin{bmatrix} 0 \\ 0 \\ 0 \\ 0 \end{bmatrix}, \begin{bmatrix} 0 \\ 0 \\ 0 \\ 0 \end{bmatrix}. \quad (6.4)$$

So $\nabla_{w,d}\phi_{0i} = 0\mathbf{w}_1 + 0\mathbf{w}_2 + 0\mathbf{w}_3 + 0\mathbf{w}_4, i = 2, 3, 4$. For these three new WG basis functions (X, Y, XY) , they are not constants. But their discrete weak gradients are zero vectors. Recall the first property in the paper [28, pg.107]:

If $\nabla_{w,d}v = 0$ on the element, then one must have $v \equiv \text{constant}$ on the element.

In other words, $v^\circ = v^\partial = \text{constant}$.

We can see that $\text{WG}(Q_1, P_1; RT_{[0]})$ does not satisfy this property.

On each element of the mesh, we compute its element stiffness matrix as follows,

$$\left[\begin{array}{c} (\mathbf{K}\nabla_{w,d}\phi_i, \nabla_{w,d}\phi_j) \end{array} \right]. \quad (6.5)$$

For a simple case $\mathbf{K} = \mathbf{I}_2$, we have found that the interaction among the discrete weak gradients of the WG basis functions for the element interior has the following structure

$$\begin{bmatrix} * & 0 & 0 & 0 \\ 0 & 0 & 0 & 0 \\ 0 & 0 & 0 & 0 \\ 0 & 0 & 0 & 0 \end{bmatrix}, \quad (6.6)$$

where $*$ is a non-zero entry.

Then we use the element stiffness matrices to construct the global stiffness matrix. On a 2×2 rectangular mesh, the global stiffness matrix is 40×40 . The 16×16 block in the

top-left corner of the matrix represents the interaction among the WG basis functions for element interiors. We have a block diagonal structure here. Each block on the diagonal is a 4×4 matrix with the structure shown in Equation (6.6). Since the discrete weak gradients in different element interiors do not interact with each other, the other parts of this 16×16 block are zeros. From previous discussion, the discrete weak gradient of any of these new WG basis functions is zero, then the interaction between this discrete weak gradient and the discrete weak gradient of any edge basis function is also zero. So in this global stiffness matrix, there is at least one row that is entirely zero. Enforcing Dirichlet boundary conditions will not affect this row, since it corresponds to an interior basis function. Thus the determinant of the global stiffness matrix is zero, and it is a singular matrix.

6.1.2 $WG(Q_0, Q_0; RT_{[1]})$ Elements on Quadrilaterals

We have seen the application of the lowest order Raviart-Thomas space in construction of WG finite elements, so we want to explore use of higher order RT spaces, e.g., $RT_{[1]}$.

Definition. Consider a rectangular element, for a non-negative integer k , the Raviart-Thomas space $RT_{[k]}$ is defined as

$$RT_{[k]} = (Q_k)^2 + \mathbf{x}Q_k, \quad (6.7)$$

where Q_k is the space of Q -type polynomials with degrees no larger than k , \mathbf{x} is a two-dimensional vector. It could also be written as

$$RT_{[k]} = P_{k+1,k} \times P_{k,k+1}, \quad (6.8)$$

where

$$P_{k+1,k} = \sum_{i=0}^{k+1} \sum_{j=0}^k a_{ij} x^i y^j, \quad P_{k,k+1} = \sum_{i=0}^k \sum_{j=0}^{k+1} a_{ij} x^i y^j.$$

Clearly, $\dim RT_{[k]} = 2(k+1)(k+2)$.

For example, when $k = 1$, $\dim RT_{[k]} = 12$, the Raviart-Thomas space is

$$RT_{[1]} = \text{Span} \{ \mathbf{w}_1, \mathbf{w}_2, \mathbf{w}_3, \mathbf{w}_4, \mathbf{w}_5, \mathbf{w}_6, \mathbf{w}_7, \mathbf{w}_8, \mathbf{w}_9, \mathbf{w}_{10}, \mathbf{w}_{11}, \mathbf{w}_{12} \}, \quad (6.9)$$

where

$$\begin{aligned} \mathbf{w}_1 &= \begin{bmatrix} 1 \\ 0 \end{bmatrix}, \quad \mathbf{w}_2 = \begin{bmatrix} 0 \\ 1 \end{bmatrix}, \quad \mathbf{w}_3 = \begin{bmatrix} X \\ 0 \end{bmatrix}, \quad \mathbf{w}_4 = \begin{bmatrix} 0 \\ Y \end{bmatrix}, \\ \mathbf{w}_5 &= \begin{bmatrix} 0 \\ X \end{bmatrix}, \quad \mathbf{w}_6 = \begin{bmatrix} Y \\ 0 \end{bmatrix}, \quad \mathbf{w}_7 = \begin{bmatrix} X^2 \\ 0 \end{bmatrix}, \quad \mathbf{w}_8 = \begin{bmatrix} XY \\ 0 \end{bmatrix}, \\ \mathbf{w}_9 &= \begin{bmatrix} X^2Y \\ 0 \end{bmatrix}, \quad \mathbf{w}_{10} = \begin{bmatrix} 0 \\ Y^2 \end{bmatrix}, \quad \mathbf{w}_{11} = \begin{bmatrix} 0 \\ XY \end{bmatrix}, \quad \mathbf{w}_{12} = \begin{bmatrix} 0 \\ XY^2 \end{bmatrix}, \end{aligned}$$

and (x_c, y_c) is the center of the quadrilateral element E , $X = x - x_c$, $Y = y - y_c$.

$\text{WG}(Q_0, Q_0; RT_{[1]})$ means that all WG basis functions are degree 0 polynomials and their discrete weak gradients are in $RT_{[1]}$. Comparing $\text{WG}(Q_0, Q_0; RT_{[1]})$ with $\text{WG}(Q_0, Q_0; RT_{[0]})$, we note that the first four basis functions of $RT_{[1]}$ are the same as the basis functions of $RT_{[0]}$. So for a WG basis function ϕ , the top four components of the right hand sides in Equation (6.2) are the same, when $RT_{[0]}$ or $RT_{[1]}$ is used.

Then we use the element stiffness matrices to construct the global stiffness matrix and solve the Darcy equation using $\text{WG}(Q_0, Q_0; RT_{[1]})$ in a similar fashion to Section 3.4.

Here, we perform a numerical test on a popular example. The exact pressure is $p = \sin(\pi x) \sin(\pi y)$ in the domain $\Omega = (0, 1)^2$. We test it on rectangular meshes. The following figures show numerical pressure and velocity obtained from using $\text{WG}(Q_0, Q_0; RT_{[1]})$.

We can see from Figure 6.2 that as the mesh is refined, the maximum of the numerical pressure is still about 0.16, but the maximum of the exact pressure should be 1. So this WG method is not suitable for solving the Darcy equation. It is possible that this combination violates the first property in [28, pg.107]. This needs further theoretical investigation.

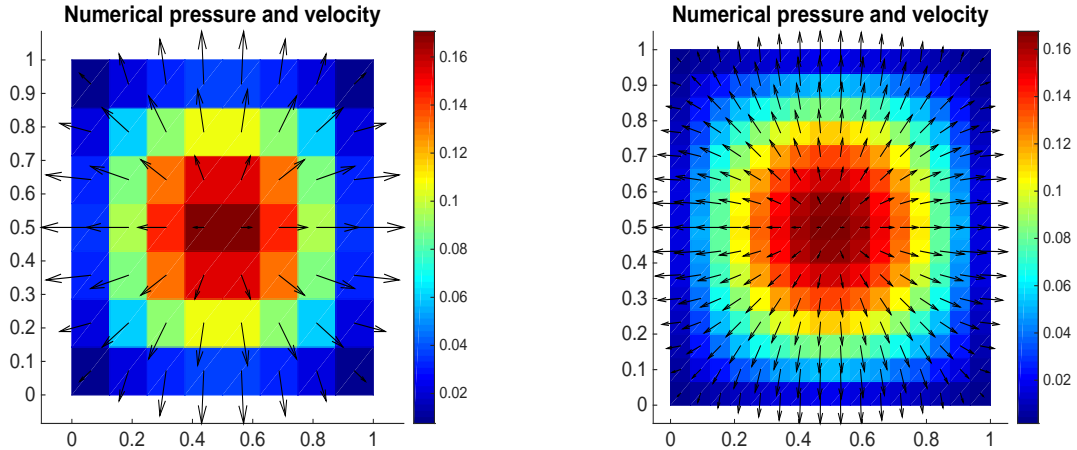


Figure 6.2: Numerical pressure and velocity obtained from using $WG(Q_0, Q_0; RT_{[1]})$ on rectangular meshes, with mesh size $h = 1/8$ and $h = 1/16$, respectively.

6.2 CONCLUSION

In this thesis, we have described development and implementation of the lowest order WGFEMs for solving the Darcy equation. We have compared this new approach to two well known methods, CGFEMs and MFEMs. The WG method is based on the novel ideas of using discrete weak functions to approximate the pressure and discrete weak gradients to approximate classical gradients. We have considered triangular and quadrilateral meshes. Rectangular meshes are treated as a special case of quadrilateral meshes. We have presented numerical results on quadrilateral meshes and hybrid meshes, which are combinations of quadrilateral and triangular elements. And expected convergence rates are obtained with mesh refinements. We have also discussed the extension of WGFEMs to three-dimensional domains. Except for the lowest order WGFEMs, we discussed two other possible WGFEMs.

In comparison to CGFEMs and MFEMs, WGFEMs have nice features, including

- Local mass conservation,
- Bulk normal flux continuity,
- SPD linear systems.

Numerical experiments suggest that WGFEMs form a new family of efficient and robust solvers for the Darcy equation.

Similar to the discrete weak gradients, discrete weak divergence and discrete weak curl can also be established. In our future work, we will develop WGFEMs to solve the elasticity equation and poroelasticity problems.

BIBLIOGRAPHY

- [1] H.-T. Ahn and G. Carey. An enhanced polygonal finite-volume method for unstructured hybrid meshes. *Int. J. Numer. Meth. Fluids*, 54:29–46, 2007.
- [2] J. Albery, C. Carstensen, and S. Funken. Remarks around 50 lines of Matlab: short finite element implementation. *Numer. Algor.*, 20:117–137, 1999.
- [3] T. Arbogast and M. R. Correa. Two families of H(div) mixed finite elements on quadrilaterals of minimal dimension. *SIAM J. Numer. Anal.*, 54:3332–3356, 2016.
- [4] D. Arnold, D. Boffi, and R. Falk. Approximation by quadrilateral finite elements. *Math. Comput.*, 71:909–922, 2002.
- [5] D. Arnold, D. Boffi, and R. Falk. Quadrilateral H(div) finite elements. *SIAM J. Numer. Anal.*, 42:2429–2451, 2005.
- [6] C. Bahriawati and C. Carstensen. Three Matlab implementations of the lower-order Raviart-Thomas MFEM with a posteriori error control. *Comput. Meth. Appl. Math.*, 5:333–361, 2005.
- [7] P. Bastian and B. Riviere. Superconvergence and $h(\text{div})$ projection for discontinuous galerkin methods. *Int. J. Numer. Meth. Fluids*, 42:1043–1057, 2003.
- [8] F. Brezzi and M. Fortin. *Mixed and hybrid finite element methods*. Springer-Verlag, 1991.
- [9] L. Bush and V. Ginting. On the application of the continuous Galerkin finite element method for conservation problems. *SIAM J. Sci. Comput.*, 35:A2953–A2975, 2013.
- [10] L. Chen. iFEM: An integrated finite element methods package in Matlab. *Technical Report, University of California at Irvine*, 2009.

- [11] S.-H. Chou and S. He. On the regularity and uniformness conditions on quadrilateral grids. *Comput. Meth. Appl. Mech. Engrg.*, 191:5149–5158, 2002.
- [12] B. Cockburn, J. Gopalakrishnan, and H. Wang. Locally conservative fluxes for the continuous Galerkin method. *SIAM J. Numer. Anal.*, 45:1742–1770, 2007.
- [13] L. Durlofsky. Accuracy of mixed and control volume finite element approximations to Darcy velocity and related quantities. *Water Resour. Res.*, 30:965–973, 1994.
- [14] R. E. Ewing. *The mathematics of reservoir simulation*. SIAM, 1983.
- [15] R. E. Ewing, M. M. Liu, and J. Wang. Superconvergence of mixed finite element approximations over quadrilaterals. *SIAM J. Numer. Anal.*, 36:772–787, 1999.
- [16] G.B.Folland. *Real analysis: Modern techniques and their applications*. 1999.
- [17] V. Ginting, G. Lin, and J. Liu. On application of the weak Galerkin finite element method to a two-phase model for subsurface flow. *J. Sci. Comput.*, 66:225–239, 2016.
- [18] G. Harper, J. Liu, and B. Zheng. The THex algorithm and a simple Darcy solver on hexahedral meshes. *Proc. Comput. Sci.*, pages Preprint, Colorado Sate University, 2017.
- [19] V. John. *Finite element methods for incompressible flow problems*. Springer, 2016.
- [20] G. Lin, J. Liu, L. Mu, and X. Ye. Weak galerkin finite element methdos for darcy flow: Anistropy and heterogeneity. *J. Comput. Phys.*, 276:422–437, 2014.
- [21] G. Lin, J. Liu, and F. Sadre-Marandi. A comparative study on the weak Galerkin, discontinuous Galerkin, and mixed finite element methods. *J. Comput. Appl. Math.*, 273:346–362, 2015.
- [22] J. Liu, L. Mu, and X. Ye. A comparative study of locally conservative numerical methods for darcy’s flows. *Proc. Comput. Sci.*, 4:974–983, 2011.

- [23] J. Liu, F. Sadre-Marandi, and Z. Wang. DarcyLite: A Matlab toolbox for Darcy flow computation. *Procedia Computer Science*, 80:1301–1312, 2016.
- [24] J. Liu, S. Tavener, and Z. Wang. The lowest-order weak galerkin finite element method for the darcy equation on quadrilateral and hybrid meshes. *Submitted*.
- [25] L. Mu, J. Wang, and X. Ye. Weak galerkin finite element methdos on polytopal meshes. *Int. J. Numer. Anal. Model.*, 12:31–53, 2015.
- [26] L. Mu, J. Wang, and X. Ye. A weak Galerkin finite element method with polynomial reduction. *J. Comput. Appl. Math.*, 285:45–58, 2015.
- [27] S. Sun and J. Liu. A locally conservative finite element method based on piecewise constant enrichment of the continuous Galerkin method. *SIAM J. Sci. Comput.*, 31:2528–2548, 2009.
- [28] J. Wang and X. Ye. A weak Galerkin finite element method for second order elliptic problems. *J. Comput. Appl. Math.*, 241:103–115, 2013.
- [29] J. Wang and X. Ye. A weak galerkin mixed finite element method for second order elliptic problems. *Math. Comput.*, 2014.
- [30] M. Wheeler, G. Xue, and I. Yotov. A multipoint flux mixed finite element method on distorted quadrilaterals and hexahedra. *Numer. Math.*, 2012.
- [31] M. Wheeler and I. Yotov. A multipoint flux mixed finite element method. *SIAM J. Numer. Anal.*, 44:2082–2106, 2006.
- [32] T. Wihler and B. Riviere. Discontinuous Galerkin methods for second-order elliptic pde with low-regularity solutions. *J. Sci. Comput.*, 46:151–165, 2011.